Quaternary Science Reviews 372 (2026) 109711

Contents lists available at ScienceDirect

Quaternary Science Reviews

journal homepage: www.elsevier.com/locate/quascirev

Assessing Atlantic subpolar gyre influence on the northern North Sea during the Holocene: A marine palaeoenvironmental reconstruction from the Fetlar basin (Shetland, UK)

Jane L. Earland [a,*], Sev Kender [a], Bernd Schöne [b], Torsa Sengupta [a], Sophie L. Ward [c], Sarah L. Bradley [d], Maarten Blaauw [e], Philippa Ascough [f], James D. Scourse [a]

[a] Department of Earth and Environmental Science, University of Exeter Penryn Campus, Cornwall, UK
[b] Institute of Geosciences, University of Mainz, Johann-Joachim-Becher-Weg 21, 55128, Mainz, Germany
[c] School of Ocean Sciences, Bangor University, Menai Bridge, Isle of Anglesey, Wales, LL59 5AB, UK
[d] Department of Geography, University of Sheffield, Sheffield, UK
[e] The ^{14}CHRONO Centre for Climate, the Environment and Chronology, Geography, Archaeology and Palaeoecology, School of Natural and Built Environment, Queen's University Belfast, Belfast, UK
[f] NEIF Radiocarbon Laboratory, SUERC, Rankine Avenue, East Kilbride, G75 0QF, UK

ARTICLE INFO

Handling Editor: Carin Andersson Dahl

Keywords:
Palaeoceanography
Late glacial
Holocene
Subpolar gyre
North Atlantic
Foraminifera
North sea
Organic carbon
Shetland Islands

ABSTRACT

Knowledge of the variability of Atlantic water inflow is critical for understanding the hydrography and ecology of the northern North Sea. However, long term records of this variability, which can be used to refine model projections of future environmental change in the region, are limited. The Fetlar Basin, located to the east of the Shetland Islands (UK), is a depositional basin situated at the intersection of the North Atlantic and northern North Sea, making it ideally placed for studying variability in Atlantic inflow. Datasets have been generated from a marine sediment core spanning the Late glacial and Holocene (c. 13 k cal a BP to present), including benthic foraminiferal assemblages, stable isotopes ($\delta^{18}O$ and $\delta^{13}C$ of *Quinqueloculina seminulum*), grain size, and sediment total organic carbon. Cluster and principal component analyses of benthic foraminiferal assemblages enabled the definition of five foraminiferal zones. The two basal zones (c. 12.9–11.0 k cal a BP) contain cold water, sea ice and glaci-proximal species typical of the Late glacial, as well as high abundances of juvenile forms. A transition from cool to warmer Holocene conditions occurs from c. 11.5 k cal a BP in a well-mixed water column. During the mid Holocene, high abundances of *F. fusiformis* are coincident with lower $\delta^{18}O$. These coincide with the Mid Holocene Climatic Optimum, and or indicate fresher, more nutrient rich water associated with higher contributions of Modified North Atlantic Water in relation to an expansion of the subpolar gyre. From c. 4.2 k cal a BP to the present, foraminiferal $\delta^{18}O$ values indicate cooler and potentially more saline conditions, which align with a general late Holocene cooling pattern in Northern Europe, and or increasing salinity due to a retraction of the subpolar gyre. Our findings provide potential long-term evidence for recent studies which emphasize the role of subpolar gyre variability in regulating North and Norwegian Sea salinity. This variability should thus be considered in the modelling and management of this region.

1. Introduction

The palaeoenvironmental history of the North Sea has been widely studied in the context of the last glacial period, up to c. 14ka BP, with significant research focusing on ice sheet dynamics and glacial retreat (Bradwell et al., 2019; Graham et al., 2010; Roberts et al., 2018, 2019). However, our understanding of the Late glacial and Holocene palaeoceanography of this region remains limited. This is in part due to the relatively low sedimentation rates that characterize much of the North Sea during the Holocene, which make it challenging to obtain continuous, high-resolution records of past environmental changes. As a result, our knowledge of the region's physical and ecological response to broader climatic and oceanographic shifts over the Late glacial and Holocene is limited.

* Corresponding author.
E-mail address: je391@exeter.ac.uk (J.L. Earland).

https://doi.org/10.1016/j.quascirev.2025.109711
Received 28 February 2025; Received in revised form 7 November 2025; Accepted 12 November 2025
Available online 20 November 2025

Modern observations and modelling suggest that the inflow of North Atlantic water plays a key role in preconditioning the physical properties of the North Sea, such as stratification, salinity, and temperature, as well as influencing the distribution of marine species in the area (Holt et al., 2018; Huthnance et al., 2016; Koul et al., 2019; Núñez-Riboni and Akimova, 2017; van der Molen and Pätsch, 2022). This Atlantic water enters the northern North Sea via three primary pathways: the Fair Isle Current (FIC), the East Shetland Atlantic Inflow (ESAI), and the Norwegian Trench Atlantic Inflow (NTAI) (Winther and Johannessen, 2006). Variability in the strength and salinity of the FIC, ESAI and NTAI has been linked to broader climatic and oceanographic features such as the North Atlantic Oscillation (NAO) (Koul et al., 2019; Winther and Johannessen, 2006) and the subpolar gyre (SPG) (Koul et al., 2019).

While these modern insights are critical for understanding the present-day conditions of the North Sea, the influence of past variability in Atlantic water is less well understood. Most reconstructions of Atlantic water variability in the eastern North Atlantic are derived from sites outside the North Sea, such as planktonic foraminiferal isotope records from the Faroe-Shetland Channel (Staines-Urías et al., 2013) and neodymium isotopes from corals in the Rockall Trough (Colin et al., 2019). These studies suggest dominance of fresher Modified North Atlantic Water (MNAW) during the early to mid Holocene, then a transition to increased presence of more saline Eastern North Atlantic Water (ENAW) in the later Holocene. Shifts in the contribution of these water masses to North Atlantic water composition have been linked to the expansion and contraction of the SPG and align with records from

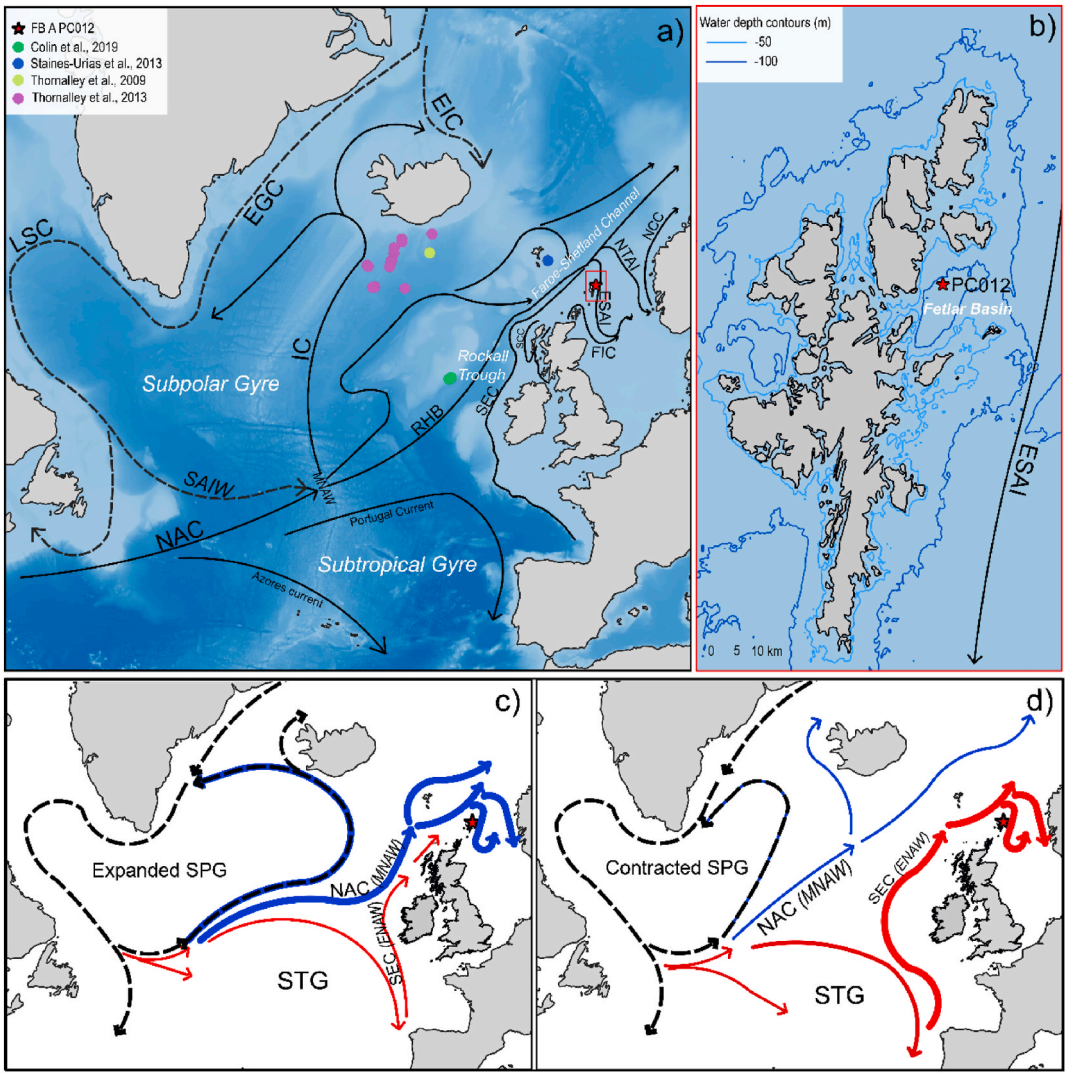

Fig. 1. a) Overview of North Atlantic currents and core sites referred to later in text. The North Atlantic Current (NAC) flows northwards and meets Sub-Antarctic Intermediate Water (SAIW), which is cooler and fresher, to form Modified North Atlantic Water (MNAW). The NAC splits at this point; one branch flows north to form the Irminger Current (IC), a northerly limb of the subpolar gyre (SPG), another branch flows northeast into the Iceland-Faroe ridge, and third flows into the Rockall Trough, known as the Rockall Hatton Branch (RHB). Other limbs of the SPG are formed by the East Greenland Current (EGC) and Labrador Sea Current (LSC). Eastern North Atlantic Water (ENAW) flows from the Bay of Biscay northwards along the Northwest European Continental Shelf via the Shelf Edge Current (SEC), into the Faroe Shetland Channel (FSC). North Atlantic water enters the North Sea via three currents, the Fair Isle Current (FIC), the East Shetland Atlantic Inflow (ESAI), and the Norwegian Trench Atlantic Inflow (NTAI). The FIC consists of a mix of North Atlantic water and Scottish coastal water from the Scottish Coastal Current (SCC). Locations of cores mentioned in the discussion (south of Iceland (Thornalley et al., 2013, 2009), the Rockall Trough (Colin et al., 2019) and the Faroe-Shetland Channel (Staines-Urías et al., 2013)) are displayed with circular points. Details of these cores can be seen in Supplementary Table 1 b) Inset map showing location of core PC012 in the Fetlar Basin, Shetland. c) and d) are a Schematic of North Atlantic Currents with c) showing an expanded SPG) and d) a contracted SPG. Blue represents MNAW (relatively cool and fresh) and red represents ENAW (relatively warm and saline). The colours represent the dominant water mass in each region during the expanded/contracted SPG. Maps adapted from Becker and Hansen (1998); Mojtahid et al. (2021); Staines-Urías et al. (2013); Turrell et al. (1996). (For interpretation of the references to colour in this figure legend, the reader is referred to the Web version of this article.)

the wider North Atlantic (Solignac et al., 2008; Thornalley et al., 2009, 2013). However, it is unknown whether these changes were also reflected in the northern North Sea.

In this study, we construct a palaeoceanographic record of northern North Sea by analysing a continuous Late glacial and Holocene sediment core (DY150 FB A PC012) from the Fetlar Basin (East Shetland, UK), which lies adjacent to the modern day East Shetland Atlantic Inflow (Turrell, 1992; Turrell et al., 1996). This site is particularly well-suited for palaeoceanographic research as previous studies have examined the modern distribution of foraminifera in the area, providing a valuable framework for interpreting past environmental changes (Klitgaard-Kristensen et al., 2002; Lo Giudice Cappelli et al., 2019; Murray, 2003a). Being adjacent to the coast as well as the open ocean, the sediments are sensitive to both local environmental conditions and broader Atlantic circulation patterns. This core therefore presents a unique opportunity to investigate a combination of Late glacial and Holocene environments, track North Atlantic water inflow variability, and study human-land-ocean interactions. This record also generates a marine counterpart to existing adjacent terrestrial records of environmental change from Shetland through the Late glacial and Holocene (Bennett et al., 1992; Edwards and Whittington, 1998; Hulme and Shirriffs, 1994; Kingsbury, 2017; Robinson, 2004; Whittington et al., 2003; Whittington and Edwards, 1993), and gives insights into the evolution of the marine environment on which many Mesolithic and early Neolithic communities in Shetland were dependent (Coull, 2003; Gillmore and Melton, 2011; Montgomery et al., 2013; Sheridan, 2012).

2. Oceanographic setting

The Fetlar Basin (Fig. 1) is a glacially deepened basin to the east of the Shetland Islands, approximately 170 km north of mainland UK. A previous study (Earland et al., 2024) found evidence of sediment disturbance and deposition in the basin related to the 8.2 ka BP Storegga tsunami event (Bondevik et al., 2005; Bryn et al., 2005), likely resulting from a submarine debris flow generated by backwash waves from the tsunami.

The basin lies on the edge of the East Shetland Atlantic Inflow (ESAI), one of three pathways by which North Atlantic water flows into the North Sea (Turrell, 1992; Turrell et al., 1996; Winther and Johannessen, 2006). The flow of the ESAI is relatively diffuse but nevertheless contributes a significant amount of Atlantic water inflow into the North Sea (Winther and Johannessen, 2006), and is a controlling factor in the inflow of the copepod *Calanus finmarchicus* into the North Sea (Beare et al., 2002; Gao et al., 2021). The strength of the ESAI is also positively correlated with growth of *Arctica islandica* (Witbaard, 1996).

Due to the small landmass of Shetland and the lack of major rivers on the islands, there is relatively little freshwater input to the coastal waters of eastern Shetland (Sheehan et al., 2017; Turrell et al., 1996). As such, the characteristics of the EASI, in particular salinity, are influenced by the composition of Atlantic waters on the shelf edge north of Shetland (Fig. 1a). These Atlantic waters are primarily comprised of two sources; Eastern North Atlantic Water (ENAW) and Modified North Atlantic Water (MNAW) (Koul et al., 2019; Turrell et al., 1996). ENAW flows northwards along the continental slope from the Bay of Biscay, through the Rockall Trough and into the Faroe-Shetland Channel, carried by the Shelf Edge Current (also known as Slope Current). This water is relatively warm and saline. MNAW is relatively fresh and cool, forming when Western North Atlantic Water, carried by the North Atlantic Current, is influenced by fresh, cool Sub Antarctic Intermediate Water (Harvey and Arhan, 1988; Holliday, 2003; New and Smythe-Wright, 2001; Read, 2000).

The relative contribution of MNAW and ENAW in the Faroe-Shetland Channel and Rockall Trough has been linked to the strength of the SPG (Hátún et al., 2005; Holliday, 2003; Holliday et al., 2008; Sherwin et al., 2012). Strengthening of the SPG results in an easterly expansion of the North Atlantic Current, which causes the Subpolar Front to shift southward in the eastern North Atlantic, as well as the retreat of subtropical gyre (STG) waters (e.g. ENAW) (Hátún et al., 2005). This allows more MNAW into the Faroe-Shetland Channel (Hátún et al., 2005; Thornalley et al., 2009), and results in a reduction in salinity and temperature in the region. The strength of the SPG is influenced by the relative contribution of freshwater to the Labrador Sea, and the strength of the NAO (Staines-Urías et al., 2013). During times of low freshwater input, the density gradient at the edge of the SPG is greater, resulting in increased baroclinic circulation. This leads to the SPG extending further eastwards, suppressing the influence of subtropical gyre water (e.g. ENAW) (Hátún et al., 2005; Thornalley et al., 2009). Additionally, in positive NAO conditions, increased westerly winds in the northern North Atlantic (Hurrell, 1995) cause cooling of surface waters. This deepens the mixed layer, increases baroclinic circulation and strengthens the SPG (Lohmann et al., 2009; Sarafanov, 2009). The strength of the SPG has subsequently been linked to salinity in the North Sea, due to the variability of North Atlantic water flowing into the northern North Sea via the three inflow routes (Koul et al., 2019; Pätsch et al., 2020). The strength of westerly winds, and as such the NAO, has also been noted to contribute to the control of nutrients in the Shetland region, with stronger westerly winds associated with higher nutrient levels (Pätsch et al., 2020).

3. Materials and methods

3.1. Core materials

Piston core DY150 FB A PC012 was recovered during the SEACHANGE DY150 research cruise in April 2022 at a water depth of 116 m in the Fetlar Basin, Shetland (60°30′17.22″N, 000°56′28.14″W (WGS84)) (Scourse et al., 2022). The core was sectioned into 1 m lengths on board before being split using a Geotek core splitter. Initial core logs were generated based on visual identification of lithostratigraphic units. The sedimentology of core PC012 has been previously reported in relation to the Storegga event (Earland et al., 2024). In the present study, the sedimentological characteristics are used alongside new foraminiferal assemblage, isotope and organic carbon datasets to characterize the Late glacial and Holocene environment. For detailed descriptions of the data acquisition and methodology for particle size analysis, ITRAX X-ray fluorescence, and multi-sensor core logger data, see Earland et al. (2024).

3.2. Core sampling

Subsamples 1 cm thick were initially taken at 16 cm intervals throughout the core, and used for micropaleontological (foraminiferal assemblages), total organic carbon (TOC) and grain size analysis. This provides an average age resolution of 330 years for the Holocene. Due to lower sedimentation rates in the upper part of the sequence, samples were taken at 8 cm intervals in the top 248 cm of the core to increase the resolution of benthic foraminiferal isotope data. This generates data at an average resolution of 230 years for the entire isotope record. Higher resolution samples, taken at 1 cm intervals between 204 and 243 cm were generated in Earland et al. (2024) to examine grain size variability within the tsunami deposit in greater detail. The outer 0.5 cm of all samples, adjacent to the core liner, was removed due to the potential for contamination during the coring process as the liner passed through the sediment. Samples were freeze dried for 48 h and subdivided to provide raw sediment for each subsequent analysis.

3.3. Radiocarbon dating and age modelling

The age model for core PC012 is based on 17 Accelerator Mass Spectrometry (AMS) ^{14}C age determinations. Earland et al. (2024) previously reported 13 of the ages used in the model, and three additional dates were obtained for the present study to improve the dating

resolution of the late Holocene section of the core. These samples consisted of mixed mollusc fragments (Table 1), which were washed and oven dried at 40 °C before processing. The outer 20 % of the sample surface was removed by acid hydrolysis, after which the remaining sample was completely hydrolysed to CO_2 before cryogenic purification and conversion to graphite (Ascough et al., 2024). Pre-treatment of samples was carried out at the Scottish Universities Environmental Research Centre NEIF Environmental Radiocarbon Laboratory (SUERC), and ^{14}C measurement was completed at the Keck Carbon Cycle AMS Facility, University of California (UCAMS). Sample $^{13}C/^{12}C$ ratio was measured in the accelerator mass spectrometer during ^{14}C measurement (also known as "online $\delta^{13}C''$). The resulting $^{13}C/^{12}C$ ratio therefore incorporates any isotopic effects resulting from graphitization and AMS measurement processes. This value was used to normalise the measured ^{14}C data to $\delta^{13}C$-VPDB‰ = −25 (c.f. Stuiver and Polach (1977)). Although online $\delta^{13}C$ values are appropriate to correct ^{14}C values for isotopic fractionation, these are not necessarily representative of the $\delta^{13}C$ in the original sample material and cannot be used to infer any additional information (e.g. environmental conditions). By convention, these values are therefore not reported, to avoid confusion with "offline $\delta^{13}C''$ values. One additional small sample consisting of mixed benthic foraminifera was selected to date the base of the core. This sample was dated at ETH Zurich (Christl et al., 2013; McIntyre et al., 2017).

A ΔR value of −109 ± 39 was selected for Holocene age samples, based on published values from Shetland (Lo Giudice Cappelli and Austin, 2020; Reimer and Reimer, 2001). Although the ΔR in this study is based on relatively modern material (1924), it is believed to have remained stable from approximately 5450–500 cal BP in northern Scotland (Russell et al., 2015), suggesting that applying a consistent ΔR is appropriate for all mid to late Holocene ^{14}C ages. Heaton et al. (2023) suggest that Holocene ΔR corrections are not appropriate for polar regions (outside ~ 40°S – 40°N) during glacial periods due to increased sea-ice cover. As such, variations in ΔR during the Younger Dryas (Austin et al., 2011; Bondevik et al., 2006), were corrected using ΔR values presented in Austin et al. (2011) from St Kilda (west Scotland). These were updated based on the MARINE20 curve (Heaton et al., 2020), see the supplementary information for re-calibration details. Based on this, the ΔR value of 326 ± 166 was chosen for ZURICH_1, and 152 ± 157 for UCAIMS-286688.

All ^{14}C measurements were calibrated using CALIB rev. 8 (Stuiver and Reimer, 1993), the MARINE20 calibration curve (Heaton et al., 2020) and ΔR corrections. These calibrated ages are presented in Table 1. No correction was made for the potential impact of the dead carbon effect (which can make ^{14}C ages appear older than their actual age), as research from cold seeps finds that neither biogenic or thermogenic methane has a significant effect on the age of shell material (Kazuhiro et al., 2016). The PC012 Bayesian age model was updated from Earland et al. (2024) to include the new ^{14}C ages. To complete the age modelling, raw ^{14}C ages were inputted into "rbacon" (version 3.3.1) following the approach in Blaauw and Christen (2011).

3.4. Micropalaeontology

Freeze dried samples were washed over a 63 μm sieve, and the residue >63 μm was oven dried for 24 h at 40 °C. After oven-drying, samples were split into aliquots using a metal sample splitter to obtain a sample which contained, where possible, ≥300 benthic foraminifera. The number of splits required to generate each aliquot was recorded to enable the calculation of benthic foraminifera abundance per gram of raw sediment. All benthic foraminifera within the >63 μm aliquots were picked and affixed to a micropalaeontology slide for identification. Inclusion of all forms >63 μm, rather than just the >125 μm fraction, was chosen as it is suggested to provide a more detailed and sensitive description of environmental change (Lo Giudice Cappelli and Austin, 2019). Additionally, the presence key indicator species such as *Fursenkoina fusiformis*, which is characteristic of nutrient availability and tidal fronts in shelf sea settings, is often lost when sieving at >125 μm (Alve, 2003; Scott et al., 2003; Scourse et al., 2002). In 38 out of the 48 samples, the number of planktonic species within the aliquot was recorded, and the planktonic-benthic ratio was calculated.

Where possible, benthic foraminifera were identified to species level based on the taxonomic works of Austin (1991), Feyling-Hanssen et al. (1971), Haynes (1973), Murray (2003a, 2006), and reference slide collections of Herron-Allen and Milton held at the Natural History Museum, London. Rare specimens (<1 % of the assemblage) for which a genus could not be determined were grouped under 'unidentifiable rare species'.

The presence of juvenile forms can provide important paleoenvironmental information, but these are often challenging to identify due to the underdevelopment of characteristic features. As such, these were grouped as 'unidentifiable juveniles'. When specimens were visually damaged, but still constituted more than half a foram test, and or calcified beyond identification, individuals were grouped into an 'unidentifiable damaged' category. Both 'unidentifiable juveniles' and 'unidentifiable damaged' specimens were removed from species counts before statistical analysis, but were included the total foram count. The percentage of 'unidentifiable damaged' tests was calculated as a percentage of the total foram count to serve as a preservation proxy.

After identification, relative abundance was calculated and filtered to contain only specimens that made up ≥ 2 % in at least one sample. The R package 'vegan' (Oksanen et al., 2024) was used to compute Shannon diversity (Shannon and Weaver, 1949), complete Hierarchical R-mode cluster analyses and principal component analysis (PCA). Hierarchical R-mode cluster analyses and PCA were performed using the Euclidean dissimilarity distance matrix and Ward's agglomeration method.

3.5. Benthic foraminiferal isotopes

Quinqueloculina seminulum was selected for stable isotope analysis ($\delta^{18}O$ and $\delta^{13}C$) due to being the most ubiquitous species within the core. *Q. seminulum* is an epifaunal benthic foraminifer which is widely distributed in UK shelf seas (Murray, 2006). In the seasonally stratified Celtic Sea, calcification takes place in September during the warmest water temperatures after the thermocline subsides and vertical mixing of warm surface water resumes (Scourse et al., 2004).

Individual tests were cleaned in an ultrasonic bath for 20 s using deionised water. Stable isotope analysis was performed at the Institute of Geosciences, University of Mainz, Germany, using a Thermo Fisher MAT 253 continuous flow-isotope ratio mass spectrometer coupled with a Gas Bench II. The foraminiferal carbonate weight ranged between 49 and 155 μg. Data were calibrated against a Carrara Marble (distributed by IVA Analysentechnik GmbH & Co. KG, Meerbusch, Germany; $\delta^{18}O$ = 1.91 ‰, $\delta^{13}C$ = +2.00 ‰). IAEA 603 ($\delta^{18}O$ = −2.37 ‰, $\delta^{13}C$ = +2.46 ‰) was used for quality control. Values are reported relative to the Vienna Pee-Dee Belemnite (VPDB). Based on long-term analysis of blindly measured NBS-19 (N = 421), the average 1 σ internal precision for $\delta^{18}O$ was better than 0.04 ‰, and better than 0.03 ‰ for $\delta^{13}C$ values. The average internal precision of the measured samples, based on eight injections per isotope value, equalled 0.05 ‰ and 0.02 ‰ for $\delta^{18}O$ and $\delta^{13}C$, respectively.

3.6. Total organic carbon (TOC)

Freeze-dried sediments (c. 1 g) were finely ground and treated with 1 N HCl at 50 °C in a water bath to completely remove inorganic carbonates. Subsequently, acid-treated sediments were washed with Milli-Q® water (c. 18.2 Ω-cm) by repeated mixing and decantation before being oven-dried at 50 °C. The carbonate content in the sediments was calculated by the weight loss of the dry sediments before and after the acid digestion process. Total organic carbon (TOC) was measured using a Leco CN828® (LECO Corporation, St. Joseph, Michigan, USA)

elemental analyser, with a detection limit of 0.02 %. Acid-digested ground sediment samples (c. 250 mg) were introduced into the auto-sampler, after which they were combusted by a purge of oxygen (99.99 %) at 950 °C. The evolved sample gas was carried by the continuous flow of an inert gas (99.99 % Argon) to a non-dispersive infrared cell to detect the CO_2 and measure the carbon content per the given sample weight. The internal reproducibility of the instrument, maintained by repeated measurements of Leco-certified soil standards (502-962™ and 502-697™), was better than 0.01 %. The measured carbon content of the sediment samples was then transformed to TOC per total sediment weight using the lost carbonate content.

4. Results

4.1. Radiocarbon and age models

The four new radiocarbon results (marked with an "a"), and the 13 previously reported radiocarbon ages are presented in Table 1. One age, UCIAMS-286688[b], was removed manually due to suspected reworking of older material. The age model is displayed in Fig. 2b. Sedimentation rates are c. 0.2 cm/yr at the base of the core, and begin to reduce between 9 and 8 k cal a BP. From 8 k cal a BP to the present day remain lower at c. 0.02 cm/yr (Fig. 2a).

4.2. Foraminiferal assemblages

In total, 48 samples were analysed for foraminiferal assemblages. 10 samples did not reach counts of 300 tests due to lack of material, but still yielded over 250. 128 foraminiferal taxa were identified; 106 to species level, and 22 to genus level. Of these, 55 taxa have a relative abundance of ≥2 % in at least one sample and are used for cluster analysis and PCA.

Cluster analysis was mainly used to define foraminiferal zones, and PCA was employed as an additional statistical measure to investigate the similarity between groupings and the species with which each group is associated (Fig. 3). The first four principal components (PCs) explain 89.3 % of the variance, and thus identify the main ecological gradients within the assemblage data; PC1 to PC4 explain 63.1, 15.8, 7.2, and 2.8 %, respectively. Species with positive scores for PC1 ≥ +1 standard deviation (σ) are *Lobatula lobatula*, *Fursenkoina fusiformis* and *Gavelinopsis praegeri*, whilst *Cassidulina reniforme*, *Buccella frigida* and *Buccella calida* show negative scores ≤ −1 σ. For PC2, *L. lobatula*, *Bolivina difformis* and *G. praegeri* show negative scores ≤ −1 σ, and *F. fusiformis* and *Epistominella vitrea* show positive loadings ≥ +1 σ. In PC3 *L. lobatula*, *B. difformis*, *Globocassidulina subglobosa* and *Cassidulina obtusa* show positive loadings ≥ +1 σ, and *G. praegeri*, *Textularia* sp. A and *Bolivina lowermani* show negative loadings ≤ −1 σ. In PC4, *L. lobatula*, *Elphidium clavatum*, *B. frigida* and *B. calida* show positive loadings ≥ +1 σ, whilst *B. difformis*, *G. subglobosa*, *C. reniforme* and *G. praegeri* show negative loadings ≤ −1 σ.

Five main foraminiferal zones were identified in the cluster analysis and are described in detail below. Foraminiferal Zone 5 was differentiated from the other four zones by being on its own branch.

4.2.1. Foraminiferal zone 5: c. 12.9–11.9 k cal a BP

The age model suggests that the top of this foraminiferal zone has a median age of c. 11.9 k cal a BP, and the base is at 12.9 k cal a BP. These dates indicate that this zone represents the Late glacial period, mainly the early Younger Dryas (~12,900 to 11,600 cal a BP; Cheng et al., 2020). However, there is a large modelled age range for the basal date (12.4–14.7 k cal a BP), and as such it may also encapsulate the Bølling-Allerød interstadial (c. 14,700 to 12,900 cal a BP; Rasmussen et al., 2006). Foraminiferal Zone 5 is largely associated with PC1. It is

Table 1
Radiocarbon ages for core PC012.

Publication Code	Sample depth (cm)	Material	Conventional radiocarbon age (years BP)	Radiocarbon age 1σ uncertainty	Calibrated age range 95 % (2σ) (cal a BP)
UCIAMS-281714	0.5	Shell fragments	440	35	Modern
SUERC-108546	25.1	Single valve - possibly *A. islandica*	1548	37	900–1230
UCIAMS-293546[a]	64.5	Shell fragments	2387	35	1780–2170
UCIAMS-293547[a]	92.5	Shell fragments	3607	35	3300–3670
UCIAMS-286683	159.5	Shell fragments	5568	32	5680–6080
UCIAMS-293548[a]	190.5	Shell fragments	6673	35	6900–7270
UCIAMS-281715	221.5	Shell fragments	7817	35	8040–8370
UCIAMS-281716	224.5	Shell fragments	7873	35	8090–8430
UCIAMS-281717[b]	227.5	Shell fragments	10,256	37	11,170–11,610
UCIAMS-286684	230.5	Shell fragments	8077	33	8330–8680
UCIAMS-286685	233.5	Shell fragments	8110	35	8360–8740
UCIAMS-281718	320.5	Shell fragments	9170	37	9660–10,130
SUERC-108547	463.7	Shell fragments	9967	40	10,750–11,180
UCIAMS-286686	494.5	Shell fragments	10,120	40	10,990–11,400
UCIAMS-286687	580.5	Shell fragments	10,558	37	11,570–12,100
UCIAMS-286688[b]	667.5	Mixed benthic foraminifera	12,320	52	13,140–13,950
ZURICH-1[a]	764.5	Mixed benthic foraminifera	11,555	95	12,030–12,990

[a] New data added in this study.
[b] Sample suspected to be subject of reworking.

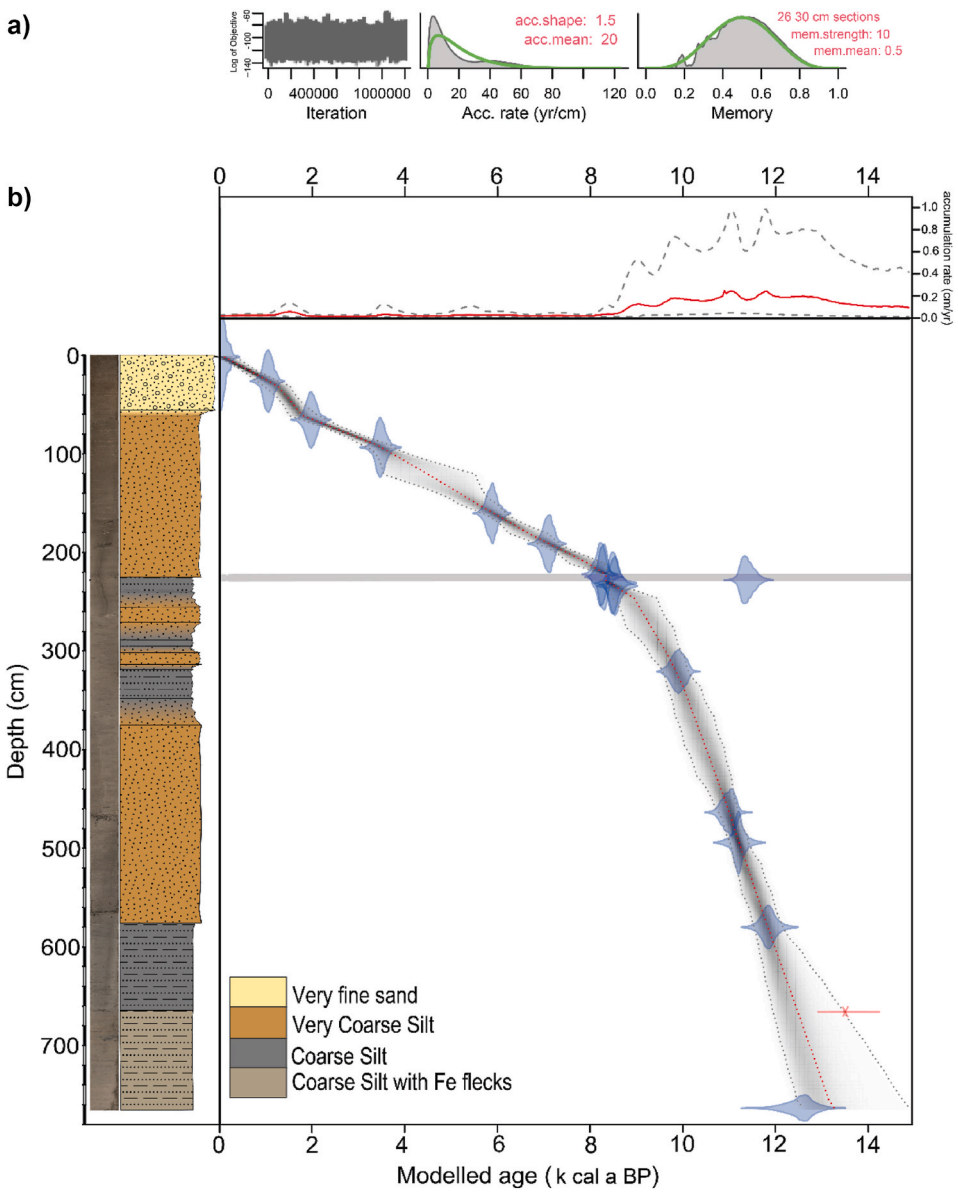

Fig. 2. a) Sediment accumulation rate for core PC012. Red line represents mean accumulation rate, dotted grey lines represent 95 % confidence interval; b) Updated age model for core PC012. Red dotted line represents the mean modelled age, and the grey dotted line represents 2σ error range. Light grey horizontal bar represents the Storegga tsunami deposit (Earland et al., 2024), modelled as slumps. Red horizontal line with a cross represent the age excluded from the age model due to suspected reworking. (For interpretation of the references to colour in this figure legend, the reader is referred to the Web version of this article.)

dominated by *C. reniforme* (37.8 % ± 10.4), with *B. calida* (12.9 % ± 5.7), *B. frigida* (10.7 % ± 5.1), *Eoeponidella pulchella* (6.9 % ± 2.7) and *E. clavatum* (6.2 % ± 2.3) as supporting species (Fig. 4). This zone also shows a high percentage of unidentifiable damaged tests, as well as low species diversity.

4.2.2. Foraminiferal zone 4: 11.9–11.0 k cal a BP

Foraminiferal Zone 4 is also dominated by *C. reniforme* (13.7 % ± 10.2) and *L. lobatula* (14.8 % ± 5.4), but *F. fusiformis* (9.9 % ± 6.4) and *E. clavatum* (8.9 % ± 4.8) are well represented species, with a contribution from *G. praegeri* (11.4 % ± 7.5) and *B. frigida* (3.7 % ± 1.9). The median values from the age model suggests this zone covers 11.9–11.0 k cal a BP, thus encompassing the mid to late Younger Dryas and transition into the early Holocene (beginning 11.5 k cal a BP; Rasmussen et al., 2006).

4.2.3. Foraminiferal zone 3: 11.0–10.2 k cal a BP

L. lobatula (24.1 % ± 4.2) and *G. praegeri* (17.7 % ± 4.3) dominate this assemblage, with *Textularia* sp. A (4.6 % ± 2.7) as an accessory. The median values from the age model suggest that the majority of this zone covers 11.0–10.2 k cal a BP. Also clustered with this zone is the 224–225 cm sample, which falls within the coarse-grained layer interpreted as a tsunami deposit by Earland et al. (2024).

4.2.4. Foraminiferal zone 2: 10.2–4.2 k cal a BP

Foraminiferal Zone 2 shows the main foraminiferal grouping for 10.2–4.2 k cal a BP. This zone is dominated by *F. fusiformis* (19.5 % ± 10.3), followed by *L. lobatula* (17.0 % ± 6.0) and *G. praegeri* (9.2 % ± 5.7). The main peak of *F. fusiformis* lies from 9.0 to 6.5 k cal a BP.

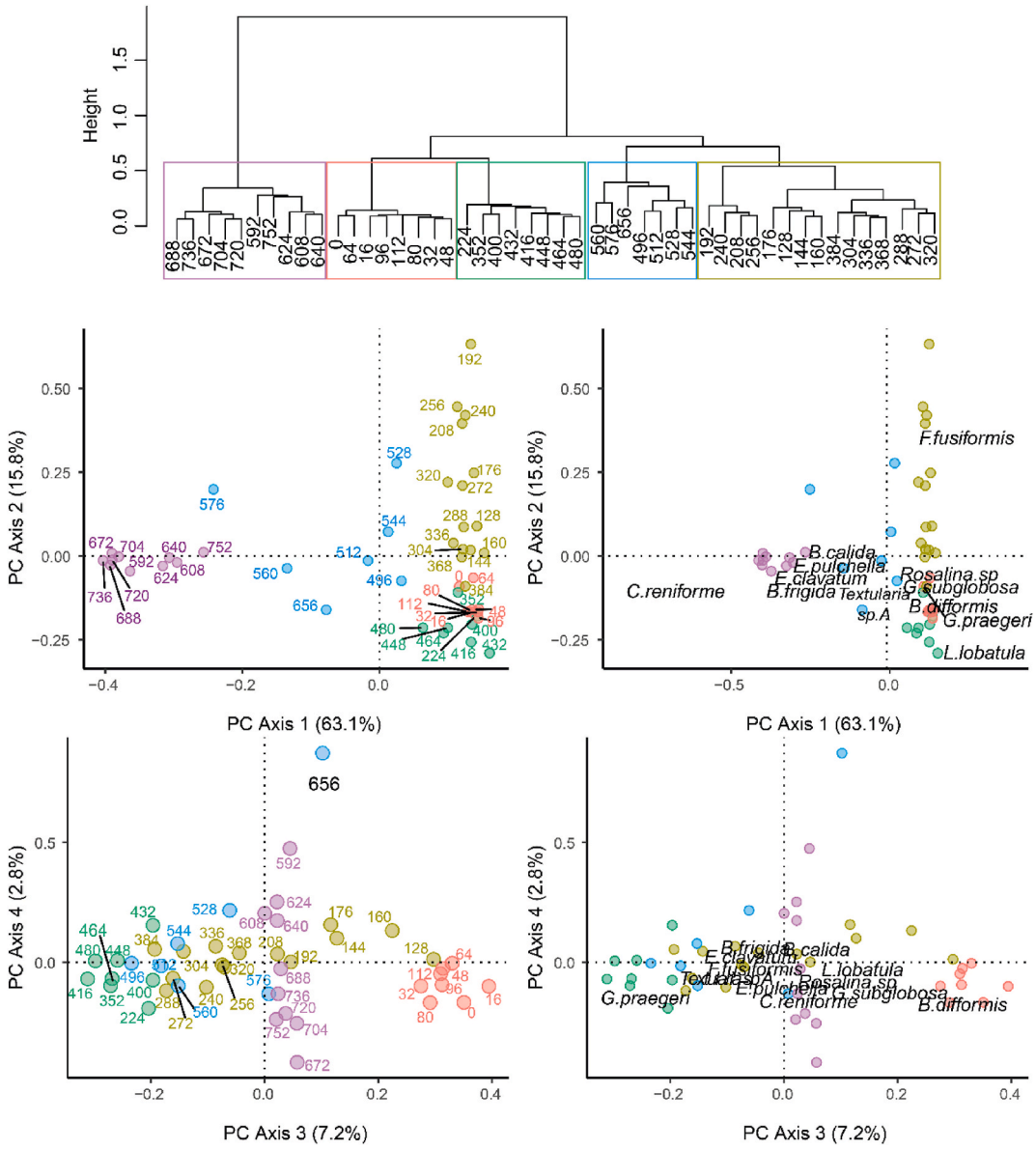

Fig. 3. Top plot – Results of cluster analysis showing foraminiferal zone groupings; Bottom plot – PCA plots showing the distributions of; left – depth (cm), and right – dominant species.

4.2.5. *Foraminiferal zone 1: 4.2 k cal a BP – present day*

Foraminiferal Zone 1 is mainly dominated by *L. lobatula* (22.9 % ± 2.5) and *B. difformis* (15.2 % ± 1). Supporting foraminifera include *G. subglobosa* (9.5 % ± 2), *G. praegeri* (8.2 % ± 2.1), *F. fusiformis* (6.8 % ± 1.3) and *Rosalina* sp (5.1 % ± 2.6). This zone largely dominates from 4.2 k cal a BP to the top of the core (present day). The main feature which differentiates this cluster from Foraminiferal Zone 2 is the dominance of *B. difformis* and *G. subglobosa*.

4.3. *Benthic foraminiferal isotopes*

Stable isotope data were obtained for 51 samples of *Q. seminulum* ranging from c. 11.6 k cal a BP to the present. Below this point there were insufficient numbers of specimens to complete analyses.

4.3.1. *Stable oxygen isotopes*

The $\delta^{18}O$ values for *Q. seminulum* ($\delta^{18}O_{foram}$) range from 0.97 to 2.54 ‰. From 11.6 to 10.5 k cal a BP, values are relatively low, but show a high degree of variability. From 10.5 to 9.0 k cal a BP, there was a transition to higher values, although these are still relatively low compared to the late Holocene. These values remain relatively constant from 9.0 to 6.0 k cal a BP. From this point, and especially from 4.2 k cal a BP onwards values become higher. The impact of the ice volume effect on $\delta^{18}O_{foram}$ values was assessed using a correction of 0.011 % $\delta^{18}O$ per m sea-level change (Fairbanks, 1989) and a relative sea level curve (Ward et al., 2025a, 2025b), but the impact on values was negligible (Supplementary Fig. 2). As such, the data presented here are not corrected for the ice volume effect.

4.3.2. *Stable carbon isotopes*

The $\delta^{13}C$ values of *Q. seminulum* ($\delta^{13}C_{foram}$) exhibited a broad range of −12.86 to 0.48 ‰. From 11.6 to 9.1 k cal a BP, some particularly negative excursions are recorded (−2.99 to −12.86 ‰) (Fig. 5). Inspection of tests visually and using Scanning Electron Microscope (Supplementary Fig. 3) did not indicate any diagenetic overgrowth that might have impacted the isotope signals. From 8.9 to 6.5 k cal a BP, values are relatively stable, and low compared to the late Holocene. From 6.5 to 4 k cal a BP, values transition to become higher and range

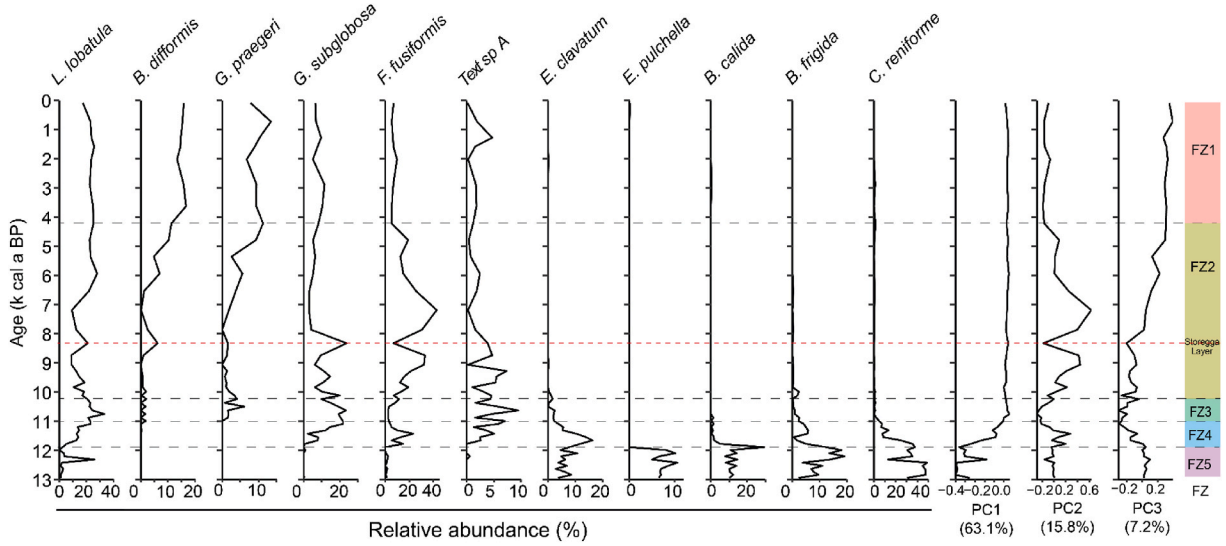

Fig. 4. Relative abundance plots of benthic foraminifera with abundance >10 % in at least two samples. PC plots show PCA scores of PC1 – 3, highlighting transitions between assemblages. Coloured bars of Foraminiferal Zones (FZ) show the change in FZ plotted against median age. Red dashed line marks assemblage from reworked Storegga Tsunami layer (Earland et al., 2024). (For interpretation of the references to colour in this figure legend, the reader is referred to the Web version of this article.

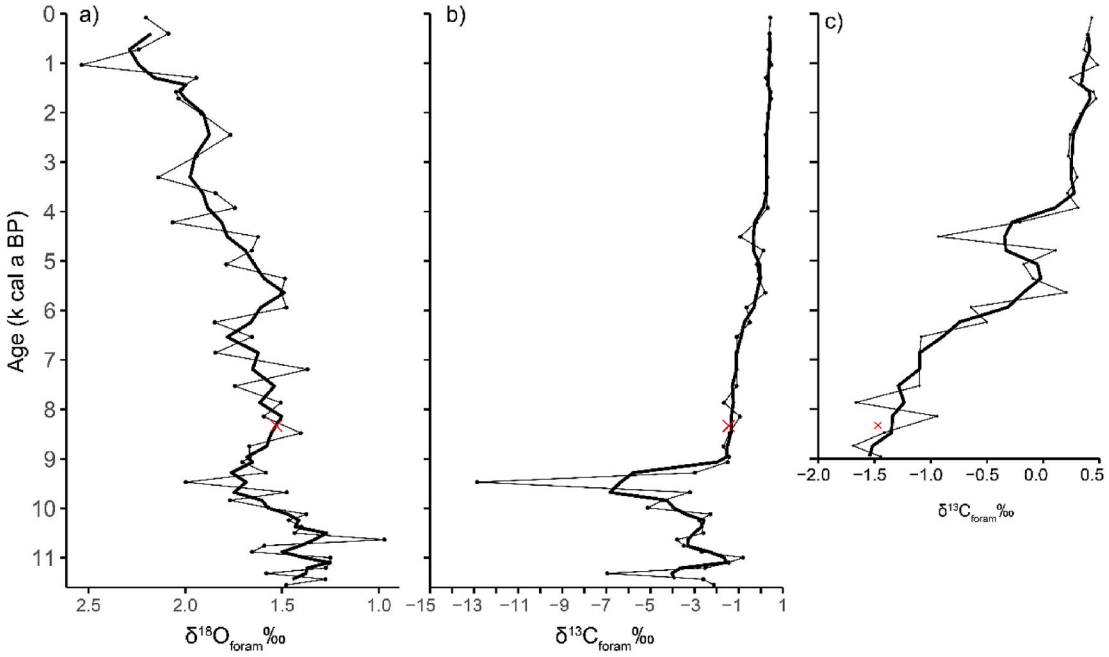

Fig. 5. Stable isotope values of *Q. seminulum*. a) The entire oxygen ($\delta^{18}O$) record, b) the entire carbon ($\delta^{13}C$) record, c) the $\delta^{13}C$ record from 9 k cal a BP to the present. Note in c) the scale has been adjusted to show the change in $\delta^{13}C$ during the Holocene, not skewed by strong negative $\delta^{13}C$ values shown in b). Three-point moving averages are shown in bold. The red cross represents data from the sample within the Storegga tsunami layer (224 – 225 cm), which is removed from the 3-point average due to potential reworking of older material (see discussion in this paper and Earland et al. (2024)). (For interpretation of the references to colour in this figure legend, the reader is referred to the Web version of this article.)

between −1.09 and 0.31 ‰. From 4 k cal a BP to the core top remain relatively high and stable.

4.4. Total organic carbon (TOC)

The TOC content for PC012 ranges between 0.31 % and 0.91 % (Fig. 6). The TOC profile can roughly be divided into five zones. From 12.9 to 12.0 k cal a BP, TOC values fall between 0.79 and 0.60 %. From 12.0 to 10.8 k cal a BP, values are lower (0.31–0.55 %). Between 10.8 and 7.2 k cal a BP, relatively high values occur again (0.63–0.91 %), with the exception of 224 cm which has a value of 0.39 %. Values remain relatively low between 7.2 and 3.6 k cal a BP, 0.46–0.53 %. From 3.6 k cal a BP to the present, TOC values rise again and range between 0.56 and 0.85 %.

5. Discussion

5.1. Late glacial 12.9–11.9 k cal a BP

Before providing a paleoenvironmental interpretation based on

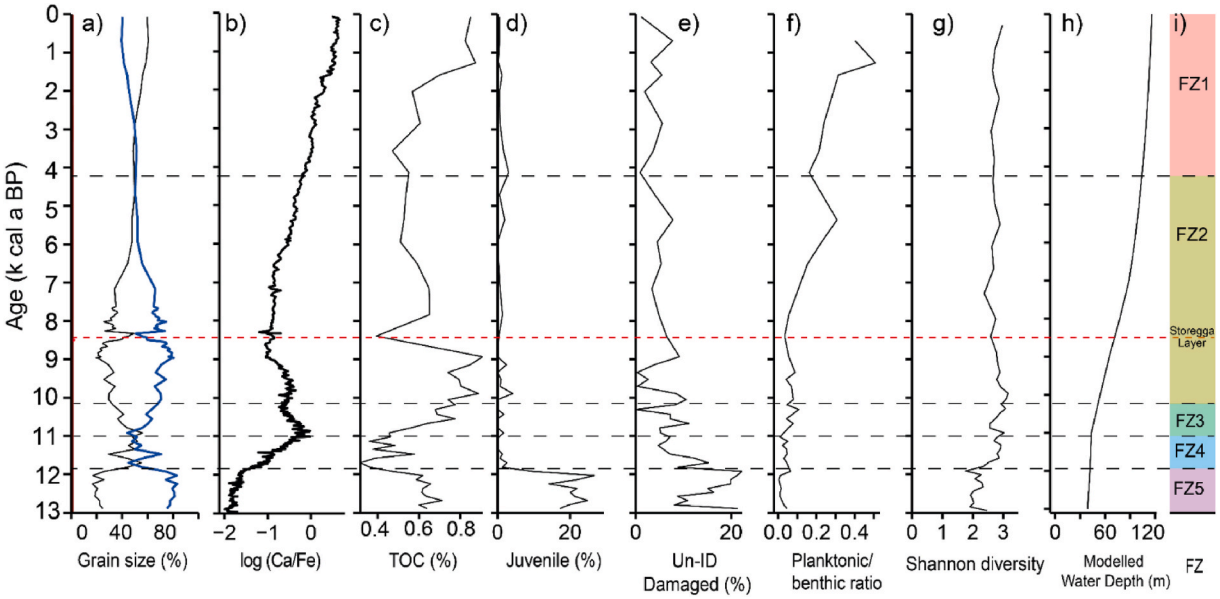

Fig. 6. Temporal changes in; a) sediment grain size distribution, red is gravel, black is sand, blue is mud; b) log (Ca/Fe) from Earland et al. (2024) down sampled to 1 cm resolution; c) total organic carbon (TOC); d) percentage juvenile forms; e) percentage of tests that were classed as "unidentifiable damaged"; f) planktonic to benthic foraminifera ratio; g) Shannon Diversity index; h) mean modelled water depth (which incorporates the relative sea level changes at the site (Ward et al., 2025b, 2025a); i) foraminiferal zones. Coloured bars for foraminiferal zones and dashed horizontal lines show the change in foraminiferal zone plotted against median age. (For interpretation of the references to colour in this figure legend, the reader is referred to the Web version of this article.)

benthic foraminiferal species, it is important to note a potential preservation bias. This is particularly the case in the Late glacial interval as it displays the highest percentage of unidentifiable damaged tests and low species diversity. In this context, high percentages of damaged calcareous tests may indicate corrosive bottom or pore waters. Corrosive waters can result from both the decomposition of high concentrations of organic flux, and the presence of brine-enriched shelf waters during periods of high sea-ice formation (Fossile et al., 2020). In this interval, TOC values are relatively high so may support the interpretation of high organic flux during this period. However, caution should be taken with this interpretation as Alve (2003) suggests that TOC may not be a good measure for periodic increases in organic flux, as benthic foraminifera may respond to fluxes of labile organic material which is not always reflected in the sedimentary TOC. This is perhaps amplified in downcore records of TOC where the percentage of labile organic matter is not measured. The low number of benthic forams/gram may also indicate generally harsh low productivity conditions associated with sea ice and glacimarine conditions (Ouellet-Bernier et al., 2014), and/or be due to dilution from high sedimentation rates (Austin, 1991). This is also supported by low log (Ca/Fe) ratios, which could indicate carbonate dissolution, or high levels of terrigenous input, which is also evident from high sedimentation rates in this period.

High agglutinated/calcareous ratios can also be indicative of corrosive bottom waters, as calcareous tests are dissolved in these contexts (Fossile et al., 2020), but very few agglutinated forms are present here. Korsun and Hald (1998) observed a similar pattern, noting that glacier-proximal assemblages in fossil records often show a dominance of *C. reniforme* and *E. clavatum*, likely due to poor agglutinated preservation. Poor preservation of fossil agglutinated foraminifera can occur as they are more subject to disaggregation by mechanical processes, compaction and degradation of the organic matter which binds tests together (Gamboa-Sojo et al., 2021; Murray, 2006; Schröder, 1988). The Late glacial here is characterised by calcareous species with relatively thick tests (*C. reniforme*, *E. clavatum*, *B. frigida* and *B. calida*). As such, the assemblage preserved may represent only the most robust calcareous tests which are the least susceptible to corrosion from bottom waters and mechanical compaction than both thinner walled hyaline species and agglutinated forms.

Despite the potential preservation bias, the Late glacial within PC012 is characterised by high percentages of *C. reniforme*, supported by *E. clavatum*, *B. frigida* and *B. calida*. *C. reniforme* is commonly found in glacimarine settings and is indicative of cold bottom water temperatures. This species is often associated with *E. clavatum* (Hald et al., 1994; Hald and Korsun, 1997; Jennings et al., 2004; Knudsen et al., 2008; Korsun and Hald, 1998; Polyak et al., 2002; Sejrup and Guilbault, 1980), another cold-water species (0–7 °C), and *B. frigida* (Murray, 1991; Rodrigues and Hooper, 1982). *E. clavatum* is an opportunistic species, well adapted to periods of fluctuating environmental conditions, making it well adapted to glacier proximal environments where changes in sediment supply and salinity are common (Jennings et al., 2004). *B. frigida* and *B. calida* are noted to bloom in different phases, with the former blooming just after the main retreat of ice, and the second during unstable sea ice conditions (Seidenkrantz, 2013). Despite this difference, both species mainly respond to increased food availability related to phytoplankton blooms on sea ice and ice margin edges. In the present study, there is no clear difference in the representation of *B. calida* and *B. frigida*, and as such the genus is in general interpreted as cold-water, opportunistic and may indicate the break-up and/or retreat of sea ice.

Foraminiferal Zone 5 shows the highest abundance of juvenile benthic foraminifera, many of which appear to be *Bucella* spp. This may indicate high reproductive activity of opportunistic species in response to phytoplankton blooms and high inputs of organic matter (Fossile et al., 2020), an interpretation supported by relatively high TOC values. Alternatively to in-situ production, juvenile propagules may have been produced elsewhere and transported by ocean currents to the core site; some benthic foraminiferal species commonly found in the North Sea produce propagules which can remain dormant for up to two years. These propagules are advected by currents, only growing if they reach an environment with suitable conditions (Alve and Goldstein, 2002, 2010). In glacimarine settings, ecologically stressful conditions, such as low food availability and rapid burial, can result in underdevelopment of forms and higher juvenile mortality. This in turn can result in a high abundance of juvenile and small forms within these settings (Korsun et al., 1995). Additionally, lower relative sea level during the Late glacial may have resulted in surface processes such as brine formation, sea ice and freezing which could have inhibited the development

juvenile forms as suggested by Mojtahid et al. (2021). This inhibition of growth would be applicable to foraminifera produced both within the Fetlar Basin and those transported from external settings.

Terrestrial evidence from Optically Stimulated Luminescence determinations of nearby moraines in central Shetland indicates that the modelled final limit for the ice mass was 14.9 ± 2.0 k cal a BP (Bradwell et al., 2019). In this context, the cold-fauna assemblage here, alongside the dominance of juveniles, may therefore be more likely associated with prevailing cold bottom waters during the Late glacial and Younger Dryas, as well as periods of sea ice cover, rather than tidewater glaciers in a glacimarine setting.

Uncertainty in the age model indicates that this core section could extend into the Bølling-Allerød warm interstadial (c. 14,700 to 12,900 cal a BP; Rasmussen et al., 2006), yet in terms of the benthic fauna in the marine record here, we see no expression of the Bølling-Allerød. However, it may be the case that warming during this interstadial did not affect bottom water temperatures. This has been shown in a high-resolution benthic foraminiferal record from the Norwegian Sea (Klitgaard-Kristensen et al., 2001), where no evidence of a benthic foraminiferal assemblage or isotopic shift during the Bølling-Allerød interstadial was recorded.

There is a lithological change during this interval at 12,380 cal a BP (666 cm), marked by much lower magnetic susceptibility values (Earland et al., 2024), a distinctly greyer colour without dark reddish-brown flecks, and the absence of thick laminations. Coincident with this lithological change is a slight positive change in PC4 (c. 0 to 0.5), which is mainly driven by *B. calida*, *B. frigida* and *L. lobatula*. This shift may represent an environmental change away from hypoxia, potentially caused by prevailing sea ice, to more oxygenated conditions, as *Bucella* spp. And *L. lobatula* are more commonly associated with higher oxygen availability (Murray, 2006; Patterson et al., 2000).

5.2. Late Younger Dryas and early Holocene 11.9–11.0 k cal a BP

The assemblage at the beginning of this period is similar to the previous zone, characterised by cold-water species. At c. 11.5 k cal BP, the assemblage begins to transition to one that is more typical of the early Holocene (section 5.3), so may represent the increasing temperatures at the beginning of the Holocene. In the centre of this zone, *E. clavatum* peaks, perhaps responding to cooler conditions during the Younger Dryas. The presence of *L. lobatula* and *G. praegeri* may relate to an increase in grain size, as these epifaunal species are found attached to coarse lithic particles (Murray, 2006). As this species inhabits a wide range of temperatures, salinities and water depths, Murray (1991) suggests the substrate is the factor which controls its distribution. Increased grain size in this period is likely the result of increased terrestrial input, as bed shear stress simulations (Ward et al., 2025a, 2025b) do not suggest high tidally induced bottom water currents in the Fetlar Basin during the early Holocene. High sedimentation rates in the early Holocene, as in PC012 (Fig. 2a), have been found in other basins on the continental shelf near Scotland (Arosio and Howe, 2018; Binns et al., 1974; Graham et al., 1990; Peacock et al., 2012), and are suggested to be the result of terrestrial landscape destabilisation during paraglacial conditions combined with a lack of development of vegetation, leading to high terrigenous sediment flux (Arosio and Howe, 2018).

The reduction in juvenile forms may indicate the presence of more favourable bottom water conditions, allowing specimens to fully develop into adult forms. The reduction in TOC is not matched by a reduction in opportunistic species; in this interval we see increased abundances of *F. fusiformis*, which show dominance associated with high organic carbon flux (Alve, 1994, 1995, 2003). The appearance of *F. fusiformis* may also be related to preservation bias rather than a change in environment; *F. fusiformis* have thin hyaline tests which are perhaps more subject to dissolution than more robust opportunistic species such as *Bucella* spp. Alternatively, *F. fusiformis* may take over as the more dominant opportunistic species as temperatures increase and cold-water opportunists such as *B. frigida* decline.

The $\delta^{18}O_{foram}$ and $\delta^{13}C_{foram}$ records initiate within this Foraminiferal Zone, at 11.6 k cal a BP. During this period, $\delta^{18}O_{foram}$ values are low compared to the mid and late Holocene. These values may reflect warmer temperatures at the beginning of the Holocene, and or a freshening of the water column related to increased meltwater during deglaciation. Increased freshwater at the surface may have promoted the development of seasonal stratification, posing another possible explanation for the presence of *F. fusiformis*, which are associated with frontal-stratified regions (Scourse et al., 2002).

The $\delta^{13}C_{foram}$ values in this interval range from −6.96 to −0.80 ‰, which is well outside the Holocene *Q. seminulum* values reported from the Celtic Sea (−0.2 to 0.6 ‰ following Scourse et al., 2002). Inspection of tests visually and using Scanning Electron Microscope (Supplementary Fig. 3) did not indicate signs of diagenetic overgrowth. If these values represent a primary (not diagenetic) signal, they may indicate the presence of methane seepage; methane seepage has been associated with low $\delta^{13}C$ values in *Q. seminulum* in the western Irish Sea (Woods et al., 2019), miliolid species in the northwest Bay of Bengal (Clemens et al., 2023), and in benthic foraminifera in the Arctic (Melaniuk et al., 2022; Panieri et al., 2014). In a palaeoceanographic context, methane seepage and subsequent negative excursions of $\delta^{13}C$ values in carbonates have been shown to occur during glacial-interglacial transitions, caused by the dissociation of gas hydrates relating to warmer temperatures and reduced pressure from ice loading (Clemens et al., 2023; Deng et al., 2021) and also during the mid Holocene (Guan et al., 2022). It is also possible that the negative $\delta^{13}C$ values in *Q. seminulum* are due to biogenic methane seepage, which occurs when anaerobic bacterial degradation of organic matter produces methane that later seeps into surrounding sediments and pore waters (Hoogakker et al., 2024). The interpretation of methane seepage affecting $\delta^{13}C_{foram}$ values is supported in this setting by pockmarks and gas fronts in sediments near to the core site (Figure 8 in Earland et al., 2024).

5.3. Early Holocene 11.0–10.2 k cal a BP

The early Holocene foraminiferal cluster is dominated by *L. lobatula* and *G. praegeri*. These species are common epifaunal shelf species living in 0–30 °C attached to coarse substrates, and are indicators of well-oxygenated bottom waters resulting from high mixing and current activity (Gasparini and Vilela, 2017; Hayward et al., 2007; Murray, 1991, 2006; Schönfeld, 2002; Scott et al., 2003). The absence of characteristically cold-water species such as *E. clavatum* and *C. reniforme* in this time interval supports interpretation of a more temperate climate on Shetland in the early Holocene (Hulme and Shirriffs, 1994; Whittington et al., 2003).

$\delta^{18}O_{foram}$ record transitions to slightly higher $\delta^{18}O_{foram}$ values from 10.5 to 9.0 k cal a BP. This period likely relates to the water column becoming more saline due to a reduction in global ice melt. $\delta^{13}C_{foram}$ values continue to show negative excursions, and are explained by the mechanisms previously discussed (Section 5.2).

5.4. Early – mid Holocene 10.2–4.2 k cal a BP

The foraminiferal assemblage in the mid Holocene is mainly characterised by increased *F. fusiformis* abundance from 9.0 to 6.5 k cal a BP. In west Shetland fjords (Lo Giudice Cappelli et al., 2019) and the Celtic Sea (Scott et al., 2003) this species is suggested to indicate stressed and perhaps stratified or frontal environments, and thus may indicate that the basin was frontal or seasonally stratified. This interpretation is supported by lower $\delta^{13}C_{foram}$ values between 9 and 6.5 k cal a BP when compared to the later Holocene (Fig. 5c); in highly productive stratified water columns, limited ventilation between surface and bottom waters results in remineralisation of $\delta^{13}C$ depleted organic matter as it passes through the thermocline. This releases depleted $\delta^{13}C$ into the water

column which is subsequently reflected in lower $\delta^{13}C_{foram}$ (Pados-Dibattista et al., 2022; Scourse et al., 2004). However, the negative excursions in $\delta^{13}C_{foram}$ prior to 9 k cal a BP make it challenging to determine if $\delta^{13}C_{foram}$ transitioned to lower values at 9 k cal a BP as a result of increased productivity, or if the water column $\delta^{13}C$ was already low. A stratified water column may also be reflected in lower log (Ca/Fe) ratios, which could indicate poorer carbonate preservation during this period (Fig. 6).

$\delta^{18}O_{foram}$ shows relatively low values from 9.0 to 5.5 k cal a BP in comparison to the later Holocene. As both water temperature and salinity affect $\delta^{18}O_{foram}$, the low values may be interpreted as either an increase in temperature, a reduction in salinity, or a combination of both factors.

During this time interval, if the basin was mixed, regular exchange with the atmosphere could result in lower $\delta^{18}O$ values linked to warmer atmospheric temperatures during the Mid Holocene Climatic Optimum (Jansen et al., 2008). However, as the $\delta^{13}C$ and assemblage data suggest that the water column was stratified, relatively low $\delta^{18}O_{foram}$ values may relate to a fresher water column in the mid Holocene, rather than reflecting the temperature.

In Shetland there is, and likely was by the mid Holocene, relatively low freshwater input (Sheehan et al., 2017; Turrell et al., 1996). As such, the $\delta^{18}O_{seawater}$ is, and likely was, primarily controlled by the salinity of the ocean water, which is in turn mainly determined by the relative contributions of ENAW (saline) and MNAW (fresher) on the slope north of Shetland. Therefore the relatively low $\delta^{18}O_{foram}$ during the mid Holocene could reflect higher contributions of MNAW. One explanation for an increase in the contribution of fresh MNAW in the region is an expansion of the SPG; some modelling studies and recent instrumental data suggest that during an easterly expansion of the SPG, salinity in the eastern North Atlantic (Fan et al., 2023; Häkkinen and Rhines, 2004; Hátún et al., 2005; Koul et al., 2020) and North Sea (Koul et al., 2019) is reduced, as less subtropical gyre water penetrates the region.

Whilst not identical, likely due to regional variation and age model differences, similarities can be seen between the east Shetland data and palaeoclimate records from the Faroe-Shetland Channel, Rockall Trough, and East Iceland Basin (Fig. 7); during the mid Holocene, commonly in the period between c. 9 and 6 k cal a BP, these records indicate a higher contribution of less saline water in the eastern SPG (Colin et al., 2019; Solignac et al., 2008; Staines-Urías et al., 2013). In the Faroe-Shetland Channel (FSC), this expansion is evidenced by lower $\delta^{18}O$ values from 7.8 to 6 k cal a BP (Staines-Urías et al., 2013), (Fig. 7c). Dinoflagellate cyst proxies from the FSC also revealed lower sea surface temperature (SST) and sea surface salinity (SSS) from 9.4 to 5.4 k cal a BP (Solignac et al., 2008). In addition, coral εNd in the SW Rockall trough (Colin et al., 2019) show values associated with unradiogenic mid-depth subpolar gyre water between 8.8 and 6.8 k cal a BP (Fig. 7d). In these records, the authors have linked their results to cooler fresh North Atlantic water flowing into the Rockall Trough and to the FSC, and/or much more cool fresh North Atlantic water flowing into the FSC from the Iceland-Faroe gap, associated with an eastward expansion of the SPG. These data also align with records for strong Iceland-Scotland Water Overflow (Fig. 7f) (Thornalley et al., 2013), which has been linked to the position of the SPG.

Fresher waters associated with an expansion of the SPG may have also contributed to stratification in the region, which supports the

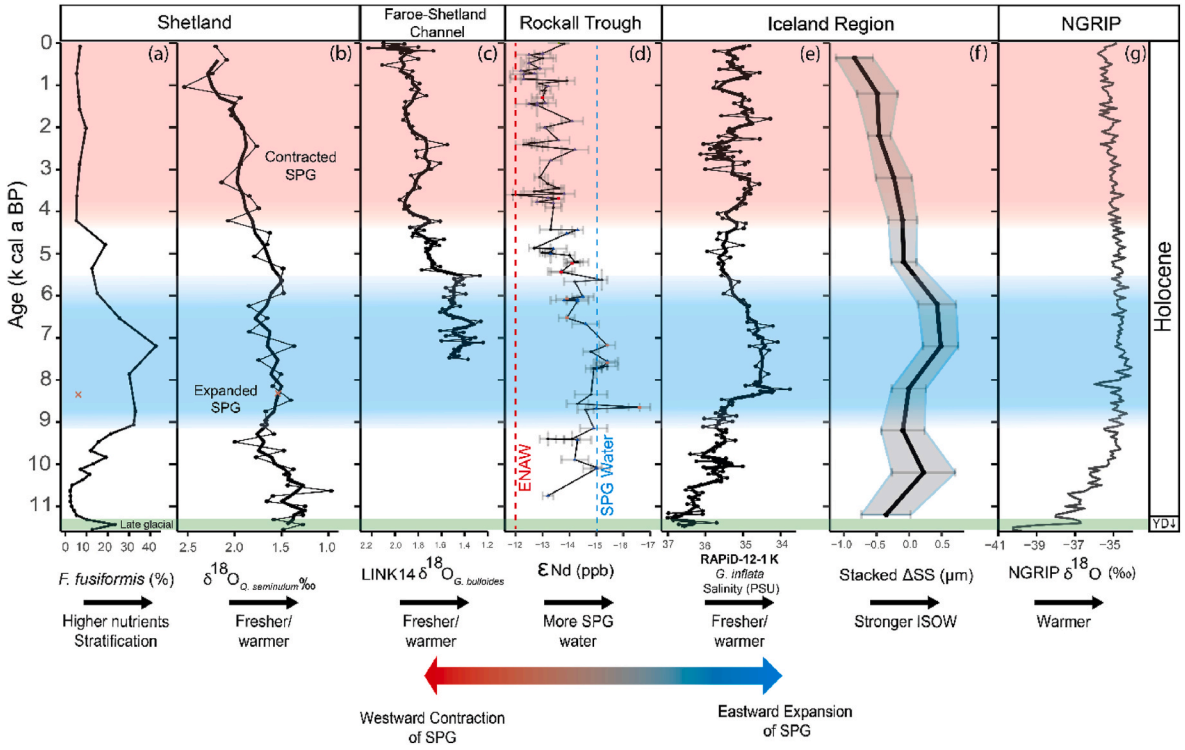

Fig. 7. Summary plot of records indicating expanded mid Holocene subpolar gyre (SPG) and contracted late Holocene SPG (a) PC012 *F. fusiformis* relative abundance; (b) PC012 $\delta^{18}O$ *Q. seminulum* with 3-point moving average. Red cross represents data from Storegga reworked layer (224 cm) excluded from trendlines; (c) *G. bulloides* $\delta^{18}O$ from the Faroe-Shetland Channel (Staines-Urías et al., 2013); (d) Neodymium isotopes from the Rockall Trough (2012-39 PC, 2013-18 PC and MD200-25BX from Colin et al. (2019), MD01-2454G from Colin et al. (2010) and Copard et al. (2012)), red dash shows ENAW Nd values, blue SPG Nd values; (e) Mg/Ca–$\delta^{18}O$ inferred salinity measurements of sub-thermocline from *G. inflata*, core RAPiD-12-1 K (south of Iceland) (Thornalley et al., 2009); (f) The stacked sortable silt (SS) data derived from multiple cores (South Iceland Rise and Bjorn Drift). The stacked dataset reflects the relative strength of the Iceland-Scotland Overflow (ISOW) (Thornalley et al., 2013). (g) The NGRIP record of atmospheric temperature (Rasmussen et al., 2006), illustrating the general atmospheric climate shift from the Younger Dryas (YD) to the Holocene. All data are presented on their original age models, and thus the plotted values may vary by 50–150 years due to updates to the marine calibration curves. (For interpretation of the references to colour in this figure legend, the reader is referred to the Web version of this article.)

abundance of *F. fusiformis* in the Shetland record. Additionally, high abundance of *F. fusiformis* may relate to higher contributions of MNAW as it is more nutrient rich than ENAW (Hátún et al., 2021). This is consistent with data which suggests that Atlantic inflows have a large influence on nutrient delivery into the North Sea (Emeis et al., 2015), and that the areas most exposed to the open ocean (such as the Shetland shelf) are most sensitive to changes in wider oceanic nutrient levels (Holt et al., 2012). Alternatively, the timing of the change in benthic assemblages may be related to the opening of the English Channel at c. 8 ka. This likely altered the hydrography of the North Sea and perhaps the benthic community, as it would have contributed to an establishment of the current North Sea circulation regime (Gyllencreutz, 2005). This is noted by Erbs-Hansen et al. (2012) in the Skagerrak, who suggested the opening of the English Channel may have contributed to an increase in *Uvigerina mediterranea,* a species linked to a strong influence of Atlantic Water and high content of organic matter, at c. 8 k cal a BP. It is interesting to note that, the peak in *F. fusiformis* subsides slightly prior to the transition to higher $\delta^{18}O_{foram}$ values; it is unclear why this is, but may be due to the lower resolution of the assemblage data.

Whilst the data in this study are supported by modelling and palaeoclimate data indicating a mid Holocene expansion of the SPG, other studies (Born et al., 2016; Foukal and Lozier, 2017; Herbaut and Houssais, 2009) do not find a relationship between salinity in the eastern North Atlantic and the size/strength of the SPG. If this is the case, changes in the proxies in this study may be the result of variation in temperature, or local changes in salinity which are yet to be understood. However, without an independent proxy for salinity, a water mass tracing proxy, or local atmospheric temperature reconstructions, it is challenging to discern whether the change in $\delta^{18}O_{foram}$ is the result of changing temperature or salinity. Thus, future studies to produce additional water mass and salinity proxies for the Fetlar Basin to strengthen the conclusions presented here.

It is also important to consider that studies which do not find a relationship between the extent of the SPG and salinity (Born et al., 2016; Foukal and Lozier, 2017; Herbaut and Houssais, 2009) may not represent long-term, millennial scale dynamics (Van Nieuwenhove et al., 2018) due to the constraints of the time periods available for model runs. Additionally, the discrepancy between model results which support and contest the relationship between the SPG extent and salinity has been shown to arise due to the differences in how SPG strength is defined, and the role of the NAO in driving changes in SPG circulation (Koul et al., 2020). To evaluate the discrepancy between these approaches, Koul et al. (2020) use multiple indices of SPG strength. They suggest that the SPG index based on the largest closed contours of SSH (as in Foukal and Lozier, 2017) fails to pick up variability because it defines the SPG boundary too narrowly, only capturing zonal changes in the western SPG, thereby excluding key variability in the eastern North Atlantic and intergyre regions. Alternatively, they suggest methods using principal component analysis of SSH and subsurface density reflect changes in the North Atlantic Current are the most suitable indices to assess subpolar gyre and water mass variability in the Eastern North Atlantic. These data support the expanded-SPG-low-salinity relationship in the eastern subpolar North Atlantic, and thus the interpretation of an expanded SPG in the mid Holocene presented here.

Some studies have suggested a link between NAO phases and the strength of the SPG (Lohmann et al., 2009; Sarafanov, 2009), and thus a comparison of NAO records and the data presented here would prove interesting. However, a comparison between the Shetland $\delta^{18}O_{foram}$ record and Holocene records of the NAO are challenging, mainly due to the variability amongst Holocene NAO records and the resolution of our data (Supplementary Fig. 5); to date reconstructions of the NAO are currently limited to only four records which span more than the last c. 2500 years (Baker et al., 2015; Becker et al., 2020; Faust et al., 2016; Olsen et al., 2012), often only showing agreement over a few specific periods. Becker et al. (2020) provide a comparison of these records, and suggests this variability potentially arises due to small catchment areas which may not fully capture NAO variability, especially as the centre shifts through time. This thus makes it challenging to draw direct comparison between the data presented here and the present NAO reconstructions, with additional limitations of the resolution meaning our data may not capture higher frequency variability related to the NAO.

5.5. Late Holocene 4.2 k cal a BP – present

The late Holocene benthic assemblage shows a return to dominance of *L. lobatula*. This assemblage is clustered closely to the early Holocene group, but as illustrated by PC3, also showed dominance of *B. difformis* and *G. subglobosa*. Overall, these species are indicative of a period of well mixed water, higher bottom water currents and dissolved oxygen, and lower levels of organic carbon (Dorst et al., 2015; Klitgaard-Kristensen et al., 2002; Lo Giudice Cappelli et al., 2019; Mackensen et al., 1995; Martins et al., 2007; Murray, 2003b; Schmiedl et al., 1997). The preference for coarse sediments amongst these foraminifera aligns with a gradual increase in grain size within the core, from very coarse silt to very fine sand. An increase in planktonic tests may indicate more oceanic influence in this interval, or increasing water depth, as planktonic forams do not live on the shelf but can be advected there by currents from the ocean (Murray, 2003b, 2004).

The isotope data show a transition to higher $\delta^{18}O_{foram}$ values after 6 k cal a BP, and especially from 4.2 k cal a BP. If this c. 0.5–0.75 ‰ increase in $\delta^{18}O_{foram}$ is entirely a reflection of changing water temperature, it would indicate a 2–3 °C drop in BWTs (Shackleton, 1974). As the benthic foraminiferal assemblage contains more mixed water species, the $\delta^{18}O_{foram}$ may be reflecting changes in temperatures in the later Holocene which show a general neoglacial cooling trend after the Mid Holocene Climatic Optimum (Kaufman et al., 2020). To confirm if this change in temperature is consistent with local air temperatures, future work to produce regional late Holocene terrestrial temperature reconstructions would be useful.

In addition to a change in temperature, reduced $\delta^{18}O_{foram}$ could reflect a change in salinity, related to an increased contribution of ENAW. A westerly contraction of the SPG may be posed as one hypothesis to explain the change in salinity, as studies have suggest that more saline ENAW is present in the region during a contracted SPG (Fan et al., 2023; Häkkinen and Rhines, 2004; Hátún et al., 2005; Koul et al., 2019, 2020). The presence of *G. subglobosa* and *L. lobatula* in our record during this interval is consistent with lower nutrient levels; ENAW being depleted in nutrients compared to MNAW is interpreted to be the reason for the upper layers in the northeast Atlantic being poorer in nutrients during a contracted subpolar gyre (Hátún et al., 2017; Johnson et al., 2013).

Similarly high $\delta^{18}O_{foram}$ values are observed in planktonic foraminifera from the Faroe-Shetland Channel during the last 4.2 ka, and values aligned more closely with the ENAW than the MNAW (Staines-Urías et al., 2013). Neodymium isotope records from corals in the SW Rockall Trough (Colin et al., 2019) also show from 7 to 5 ka a relatively smooth transition from subpolar gyre to subtropical gyre (ENAW) sourced water. These palaeoclimate records provide context and support for the change observed here in the late Holocene.

As discussed in Section 5.4, the relationship between salinity in the eastern SPG region is contested by some studies. Nevertheless, when compared to other regional palaeoclimate records, and the fact that salinity on the shelf north of Shetland is controlled by wider oceanographic forcings, our data can reasonably be interpreted to be consistent with published suggestions of a mid Holocene expansion, late Holocene contraction of the SPG.

The resolution of the east Shetland data prevents investigation into smaller-scale variation in SPG during the Holocene. As evidenced by other records (e.g. Colin et al., 2019), it is unlikely that the SPG has remained in a single state throughout the late Holocene. Rather, our data provide an initial investigation into broad scale palaeoceanographic change in the northern North Sea, and its potential links to wider ocean

dynamics. The study here is also not intended to propose a mechanism behind changes in the SPG observed in palaeoceanographic records presented in Fig. 7. However, detailed analysis of paleo-ocean SST data by Ayache et al. (2018) propose that a potential AMOC (and thus SPG) weakening may be related to reduction in the convective activity in the Nordic Seas and thus deepwater formation (Kissel et al., 2013). These mechanisms may provide wider context for the changes observed in the east Shetland data, but we do not attempt to confirm these hypotheses with the data in this paper.

5.6. Implications of the Storegga tsunami event

One of the samples investigated here (224 cm) lies within a coarse-grained sediment layer previously proposed by Earland et al. (2024) as a deposit from a submarine debris flow associated with the Storegga tsunami event. Radiocarbon dates from this depth are calibrated to 8090–8430 cal a BP, aligning with the timing of the Storegga event (around 8150 cal a BP) and at 227.5 cm, radiocarbon dates suggest evidence of reworking, with anomalously old ages of 11,170–11,610 cal a BP. Radiocarbon dates and sedimentology do not suggest reworking of material outside of the coarse grained layer (222–228 cm) (Earland et al., 2024), and as such do not pose palaeoceanographic concern for the surrounding sediments.

The clustering of the 224 cm sample with early Holocene sediments may support the theory of reworking and redeposition of earlier sediments and foraminifera by the submarine debris flow. Alternatively, this pattern could result from a preservation bias rather than reworked material; the 224 cm sample showed a reduction in *F. fusiformis*, a thin-walled foraminifera that may be more susceptible to dissolution due to tsunami-induced disturbance. The 224 cm assemblage did not show high abundances of shallow water foraminifera, indicating older material is likely more locally sourced than transported from the coastal zone. This contrasts offshore tsunami deposits on the Algarve Shelf (Quintela et al., 2016) and Augusta Bay (Smedile et al., 2012), where shallower water foraminifera are found in the tsunami layers. Additionally, we did not observe a high proportion of unidentifiable damaged tests. Our study illustrates the need for higher resolution studies across this interval to further understand the foraminiferal record of the Storegga event offshore Shetland.

6. Conclusion

The data presented here provide a comprehensive Late glacial and Holocene reconstruction for the northern North Sea using a marine sediment core from the Fetlar Basin (Shetland, UK). The foraminiferal assemblage data, supported by the isotopic and total organic carbon record, has characterised the setting into five main zones.

- The period 12.9–11.9 k cal a BP is marked by a high abundance of cold-water, glacial-proximal species such as *C. renifome* and *E. clavatum*, indicative of cold climatic conditions. The presence of abundant juvenile foraminifera suggests that harsh environmental conditions inhibited the development of adult forms.
- A transitional phase from 11.9 to 11.0 k cal a BP is characterised by a decline in cold-water species and shift towards mixed water, coarse sediment favouring species, such as *L. lobatula* and *G. praegeri* at 11.5 k cal a BP. This suggests an amelioration of the climate aligning with increasing temperatures at the start of the Holocene epoch.
- From 11.0 to 10.2 k cal a BP, the foraminiferal assemblage is dominated by *L. lobatula* and *G. praegeri.* This assemblage shows a relatively stable early Holocene warm andmixed water assemblage.
- The period from 10.2 to 4.2 k cal a BP is primarily defined by an increase in the presence of *F. fusiformis. F. fusiformis* may indicate the development of stratification, and/or nutrient-enriched water related to increased fresh, nutrient rich Modified North Atlantic Water. Oxygen isotopes may reflect the Mid Holocene Climatic Optimum, and potentially greater influence of relatively fresh Modified North Atlantic Water, likely related to an eastward expansion of the subpolar gyre during the mid Holocene. This interval also includes the Storegga Slide tsunami depositional layer, which clusters with the previous assemblage. This supports the interpretation of reworking and deposition of older material, or preservation of thicker walled tests.
- From 4.2 k cal a BP to the present there is an increase in the presence of *L. lobatula*, *B. difformis* and *G. subglobosa.* These species are all found in coarse sediments, in environments with relatively low organic matter and that are well-oxygenated. Oxygen isotopes may represent atmospheric neoglacial cooling, and potentially greater influence of relatively saline and nutrient poor Eastern North Atlantic Water related to a contracted subpolar gyre.

The results presented here may provide evidence for the sensitivity of North Sea salinity to the SPG throughout the mid and late Holocene. These conclusions are supported by recent modelling studies which highlight how variation in the SPG plays a critical role in regulating the salinity of the North Sea (Koul et al., 2019) and the Norwegian Sea (Fan et al., 2023). As such, future hydrography, stratification (Núñez-Riboni and Akimova, 2017) and distribution of fish stocks (Akimova et al., 2016) in the North Sea may be impacted by changes in the wider North Atlantic. However, based on the discrepancy between some modelling studies of SPG variability and salinity in the easter subpolar gyre, future work should consider producing additional proxy data to investigate the salinity and water masses in the ESAI region to strengthen our understanding of the influence of the SPG on the North Sea.

Author contributions

JLE – Conceptualization, Formal analysis, Investigation, Data curation, Writing – Original Draft, JDS – Conceptualization, Funding acquisition, Supervision, Writing – Reviewing and Editing, SK – Conceptualization, Supervision, Writing – Reviewing and Editing, BS - Investigation, Funding acquisition, Writing – Reviewing and Editing, TS – Investigation, Writing – Reviewing and Editing, SLW – Investigation, Formal analysis, Writing – Reviewing and Editing, SLB – Investigation, Formal analysis, MB – Writing – Reviewing and Editing, PA – Investigation, Writing – Reviewing and Editing.

AI statement

During the preparation of this work the author(s) used ChatGPT in order to refine code for generating plots and improving grammar. After using this tool/service, the author(s) reviewed and edited the content as needed and take(s) full responsibility for the content of the published article.

Declaration of competing interest

The authors declare no competing financial or personal relationship interests.

Acknowledgements and Funding

This project has received funding from the University of Exeter, and the European Research Council (ERC) under the European Union's Horizon 2020 research and innovation programme (grant agreement No 856488). JDS, SLW, SLB, and TS acknowledge funding from Convex Group Ltd for the Convex Seascape Survey, which is facilitated by Blue Marine Foundation (https://www.bluemarinefoundation.com/projects/convex-seascape-survey). Special thanks are given to Danielle Vosper for picking carbonate for some of the radiocarbon dates, Dr Francisca Staines-Urias for providing the LINK 14 isotope dataset, Prof. David Thornalley for providing RAPiD-12-1 K and ISOW data, and Prof.

Marit-Solveig Seidenkrantz and Dr Alix Cage for help with foraminiferal identification. Thanks also to the lab staff at the ETH Zurich, the Scottish Universities Environmental Research Centre NEIF Environmental Radiocarbon Laboratory (SUERC), East Kilbride, and Dr. Xiaomei Xu at the Keck Carbon Cycle AMS Facility, University of California, Irvine, USA for analysing radiocarbon samples. Finally, we thank the crew and shipboard party of the RRS *Discovery* DY150 research cruise for facilitating and aiding sediment core recovery. We also thank two anonymous reviewers for their helpful and constructive feedback on this work.

Appendix A. Supplementary data

Supplementary data to this article can be found online at https://doi.org/10.1016/j.quascirev.2025.109711.

Data availability

Datasets presented in this study are available in supplementary information of this article.

References

Akimova, A., Núñez-Riboni, I., Kempf, A., Taylor, M.H., 2016. Spatially-resolved influence of temperature and salinity on stock and recruitment variability of commercially important fishes in the north sea. PLoS One 11, e0161917. https://doi.org/10.1371/journal.pone.0161917.

Alve, E., 2003. A common opportunistic foraminiferal species as an indicator of rapidly changing conditions in a range of environments. Estuar. Coast Shelf Sci. 57, 501–514. https://doi.org/10.1016/S0272-7714(02)00383-9.

Alve, E., 1995. Benthic foraminiferal distribution and recolonization of formerly anoxic environments in drammensfjord, southern Norway. Mar. Micropaleontol. 25, 169–186. https://doi.org/10.1016/0377-8398(95)00007-N.

Alve, E., 1994. Opportunistic features of the foraminifer *Stainforthia fusiformis* (williamson): evidence from frierfjord, Norway. J. Micropalaeontol. 13, 24. https://doi.org/10.1144/jm.13.1.24, 24.

Alve, E., Goldstein, S.T., 2010. Dispersal, survival and delayed growth of benthic foraminiferal propagules. J. Sea Res. 63, 36–51. https://doi.org/10.1016/j.seares.2009.09.003.

Alve, E., Goldstein, S.T., 2002. Resting stage in benthic foraminiferal propagules: a key feature for dispersal? Evidence from two shallow-water species. J. Micropalaeontol. 21, 95–96. https://doi.org/10.1144/jm.21.1.95.

Arosio, R., Howe, J.A., 2018. Lateglacial to Holocene palaeoenvironmental change in the muck deep, offshore Western Scotland. Scot. J. Geol. 54, 99–114. https://doi.org/10.1144/sjg2017-014.

Ascough, P., Bompard, N., Garnett, M.H., Gulliver, P., Murray, C., Newton, J.-A., Taylor, C., 2024. 14C measurement of samples for environmental science applications at the national environmental isotope facility (NEIF) radiocarbon laboratory, SUERC, UK. Radiocarbon 1–12. https://doi.org/10.1017/RDC.2024.9.

Austin, W.E.N., 1991. Late Quaternary Benthonic Foraminiferal Stratigraphy of the Western U.K. Continental Shelf. University College of North Wales, Bangor.

Austin, W.E.N., Telford, R.J., Ninnemann, U.S., Brown, L., Wilson, L.J., Small, D.P., Bryant, C.L., 2011. North Atlantic reservoir ages linked to high younger dryas atmospheric radiocarbon concentrations. Global and Planetary Change, Rapid climate change: lessons from the recent geological past 79, 226–233. https://doi.org/10.1016/j.gloplacha.2011.06.011.

Ayache, M., Swingedouw, D., Mary, Y., Eynaud, F., Colin, C., 2018. Multi-centennial variability of the AMOC over the Holocene: a new reconstruction based on multiple proxy-derived SST records. Glob. Planet. Change 170, 172–189.

Baker, A., C Hellstrom, J., Kelly, B.F.J., Mariethoz, G., Trouet, V., 2015. A composite annual-resolution stalagmite record of north Atlantic climate over the last three millennia. Sci. Rep. 5, 10307. https://doi.org/10.1038/srep10307.

Beare, D.J., Batten, S., Edwards, M., Reid, D.G., 2002. Prevalence of boreal Atlantic, temperate Atlantic and neritic zooplankton in the north Sea between 1958 and 1998 in relation to temperature, salinity, stratification intensity and Atlantic inflow. J. Sea Res. 48, 29–49. https://doi.org/10.1016/S1385-1101(02)00131-4.

Becker, G., Hansen, B., 1998. Modified North Atlantic water. Cooperative research report-international council for the exploration of the sea 225, 96–111.

Becker, L.W.M., Sejrup, H.P., Hjelstuen, B.O., Haflidason, H., Kjennbakken, H., Werner, J.P., 2020. Palaeo-productivity record from Norwegian Sea enables north Atlantic oscillation (NAO) reconstruction for the last 8000 years. npj Clim. Atmos. Sci. 3, 1–12. https://doi.org/10.1038/s41612-020-00147-6.

Bennett, K.D., Boreham, S., Sharp, M.J., Switsur, V.R., 1992. Holocene history of environment, vegetation and human settlement on catta ness, lunnasting, shetland. J. Ecol. 80, 241. https://doi.org/10.2307/2261010.

Binns, P.E., Harland, R., Hughes, M.J., 1974. Glacial and postglacial sedimentation in the Sea of the Hebrides. Nature 248, 751–754. https://doi.org/10.1038/248751a0.

Blaauw, M., Christen, J.A., 2011. Flexible paleoclimate age-depth models using an autoregressive gamma process. Bayesian Analysis 6, 457–474. https://doi.org/10.1214/11-BA618.

Bondevik, S., Mangerud, J., Birks, H.H., Gulliksen, S., Reimer, P., 2006. Changes in north Atlantic radiocarbon reservoir ages during the allerød and younger dryas. Science 312, 1514–1517. https://doi.org/10.1126/science.1123300.

Bondevik, S., Mangerud, J., Dawson, S., Dawson, A., Lohne, Ø., 2005. Evidence for three north sea tsunamis at the shetland islands between 8000 and 1500 years ago. Quat. Sci. Rev. 24, 1757–1775. https://doi.org/10.1016/j.quascirev.2004.10.018.

Born, A., Stocker, T.F., Sandø, A.B., 2016. Transport of salt and freshwater in the Atlantic subpolar gyre. Ocean Dyn. 66, 1051–1064. https://doi.org/10.1007/s10236-016-0970-y.

Bradwell, T., Small, D., Fabel, D., Clark, C.D., Chiverrell, R.C., Saher, M.H., Dove, D., Callard, S.L., Burke, M.J., Moreton, S.G., Medialdea, A., Bateman, M.D., Roberts, D. H., Golledge, N.R., Finlayson, A., Morgan, S., Cofaigh, C., 2019. Pattern, style and timing of British–Irish ice sheet retreat: shetland and northern north sea sector. J. Quat. Sci. 36, 681–722. https://doi.org/10.1002/jqs.3163.

Bryn, P., Berg, K., Forsberg, C.F., Solheim, A., Kvalstad, T.J., 2005. Explaining the storegga slide. Mar. Petrol. Geol. 22, 11–19. https://doi.org/10.1016/j.marpetgeo.2004.12.003.

Cheng, H., Zhang, H., Spötl, C., Baker, J., Sinha, A., Li, H., Bartolomé, M., Moreno, A., Kathayat, G., Zhao, J., Dong, X., Li, Y., Ning, Y., Jia, X., Zong, B., Ait Brahim, Y., Pérez-Mejías, C., Cai, Y., Novello, V.F., Cruz, F.W., Severinghaus, J.P., An, Z., Edwards, R.L., 2020. Timing and structure of the younger dryas event and its underlying climate dynamics. Proc. Natl. Acad. Sci. U.S.A 117, 23408–23417. https://doi.org/10.1073/pnas.2007869117.

Christl, M., Vockenhuber, C., Kubik, P.W., Wacker, L., Lachner, J., Alfimov, V., Synal, H.-A., 2013. The ETH Zurich AMS facilities: performance parameters and reference materials. Proceedings of the Twelfth International Conference on Accelerator Mass Spectrometry. Nuclear Instruments and Methods in Physics Research Section B: Beam Interactions with Materials and Atoms, pp. 29–38. https://doi.org/10.1016/j.nimb.2012.03.004. Wellington, New Zealand, 20-25 March 2011 294.

Clemens, S.C., Thirumalai, K., Oppo, D., 2023. Indian margin methane hydrate dissociation recorded in the carbon isotopes of benthic (miliolida) Foraminifera. Earth Planet Sci. Lett. 609, 118101. https://doi.org/10.1016/j.epsl.2023.118101.

Colin, C., Frank, N., Copard, K., Douville, E., 2010. Neodymium isotopic composition of deep-sea corals from the NE Atlantic: implications for past hydrological changes during the Holocene. Quaternary Science Reviews, Special Theme: Case Studies of Neodymium Isotopes in Paleoceanography 29, 2509–2517. https://doi.org/10.1016/j.quascirev.2010.05.012.

Colin, C., Tisnérat-Laborde, N., Mienis, F., Collart, T., Pons-Branchu, E., Dubois-Dauphin, Q., Frank, N., Dapoigny, A., Ayache, M., Swingedouw, D., Dutay, J.-C., Eynaud, F., Debret, M., Blamart, D., Douville, E., 2019. Millennial-scale variations of the Holocene north Atlantic mid-depth gyre inferred from radiocarbon and neodymium isotopes in cold water corals. Quat. Sci. Rev. 211, 93–106. https://doi.org/10.1016/j.quascirev.2019.03.011.

Copard, K., Colin, C., Henderson, G.M., Scholten, J., Douville, E., Sicre, M.-A., Frank, N., 2012. Late Holocene intermediate water variability in the northeastern Atlantic as recorded by deep-sea corals. Earth Planet Sci. Lett. 313–314, 34–44. https://doi.org/10.1016/j.epsl.2011.09.047.

Coull, J.R., 2003. The shaping of shetland: an archipelago's landscape history. Landscapes 4, 67–91. https://doi.org/10.1179/lan.2003.4.2.67.

Deng, Y., Chen, F., Guo, Q., Hu, Y., Chen, D., Yang, S., Cao, J., Chen, H., Wei, R., Cheng, S., Zhou, J., Liu, C., Jiang, X., Zhu, J., 2021. Possible links between methane seepages and glacial-interglacial transitions in the South China Sea. Geophys. Res. Lett. 48, e2020GL091429. https://doi.org/10.1029/2020GL091429.

Dorst, S., Schönfeld, J., Walter, L., 2015. Recent benthic foraminiferal assemblages from the Celtic sea (south Western approaches, NE Atlantic). Paläontol. Z. 89, 287–302. https://doi.org/10.1007/s12542-014-0240-6.

Earland, J.L., Scourse, J.D., Ehmen, T., Kender, S., Ascough, P., 2024. Identification of the storegga event offshore shetland. Mar. Geol. 474, 107334. https://doi.org/10.1016/j.margeo.2024.107334.

Edwards, K.J., Whittington, G., 1998. Landscape and environment in prehistoric west mainland, shetland. Landsc. Hist. 20, 5–17. https://doi.org/10.1080/01433768.1998.10594498.

Emeis, K.-C., van Beusekom, J., Callies, U., Ebinghaus, R., Kannen, A., Kraus, G., Kröncke, I., Lenhart, H., Lorkowski, I., Matthias, V., Möllmann, C., Pätsch, J., Scharfe, M., Thomas, H., Weisse, R., Zorita, E., 2015. The north sea — a shelf sea in the anthropocene. J Marine Systems, Biogeochemistry-ecosystem interaction on changing continental margins in the Anthropocene 141, 18–33. https://doi.org/10.1016/j.jmarsys.2014.03.012.

Erbs-Hansen, D.R., Knudsen, K.L., Gary, A.C., Gyllencreutz, R., Jansen, E., 2012. Holocene climatic development in Skagerrak, eastern north Atlantic: foraminiferal and stable isotopic evidence. Holocene 22, 301–312. https://doi.org/10.1177/0959683611423689.

Fairbanks, R.G., 1989. A 17,000-year glacio-eustatic sea level record: influence of glacial melting rates on the younger dryas event and deep-ocean circulation. Nature 342, 637–642. https://doi.org/10.1038/342637a0.

Fan, H., Borchert, L.F., Brune, S., Koul, V., Baehr, J., 2023. North Atlantic subpolar gyre provides downstream ocean predictability. npj Clim. Atmos. Sci. 6, 1–8. https://doi.org/10.1038/s41612-023-00469-1.

Faust, J.C., Fabian, K., Milzer, G., Giraudeau, J., Knies, J., 2016. Norwegian fjord sediments reveal NAO related winter temperature and precipitation changes of the past 2800 years. Earth Planet Sci. Lett. 435, 84–93. https://doi.org/10.1016/j.epsl.2015.12.003.

Feyling-Hanssen, R.W., Jorgensen, J., Knudsen, K., 1971. Late Quaternary Foraminifera from vendsyssel, Denmark and sandnes, Norway. Bull. Geol. Soc. Den. 21, 67–71.

Fossile, E., Nardelli, M.P., Jouini, A., Lansard, B., Pusceddu, A., Moccia, D., Michel, E., Péron, O., Howa, H., Mojtahid, M., 2020. Benthic Foraminifera as tracers of brine

production in the storfjorden “sea ice factory.”. Biogeosciences 17, 1933–1953. https://doi.org/10.5194/bg-17-1933-2020.
Foukal, N.P., Lozier, M.S., 2017. Assessing variability in the size and strength of the north Atlantic subpolar gyre. J. Geophys. Res.: Oceans 122, 6295–6308. https://doi.org/10.1002/2017JC012798.
Gamboa-Sojo, V.M., Husum, K., Caridi, F., Lucchi, R.G., Bensi, M., Kovačević, V., Sabbatini, A., Langone, L., Dominiczak, A.T., Povea, P., Morigi, C., 2021. Living and dead foraminiferal assemblages of the last decades from Kveithola Trough: taphonomic processes and ecological highlights. Mar. Micropaleontol. 166, 102014. https://doi.org/10.1016/j.marmicro.2021.102014.
Gao, S., Hjøllo, S.S., Falkenhaug, T., Strand, E., Edwards, M., Skogen, M.D., 2021. Overwintering distribution, inflow patterns and sustainability of *Calanus finmarchicus* in the north sea. Prog. Oceanogr. 194, 102567. https://doi.org/10.1016/j.pocean.2021.102567.
Gasparini, S.P., Vilela, C.G., 2017. Paleoenvironmental evolution based on benthic Foraminifera biofacies of the Paraíba do sul deltaic complex, eastern Brazil. J. S. Am. Earth Sci. 80, 291–303. https://doi.org/10.1016/j.jsames.2017.09.026.
Gillmore, G.K., Melton, N., 2011. Early Neolithic sands at west voe, shetland islands: implications for human settlement. Geological Society, London, Special Publications 352 (6), 69–83. https://doi.org/10.1144/SP352.
Graham, A.G.C., Lonergan, L., Stoker, M.S., 2010. Depositional environments and chronology of late Weichselian glaciation and deglaciation in the central north sea. Boreas 39, 471–491. https://doi.org/10.1111/j.1502-3885.2010.00144.x.
Graham, D.K., Harland, R., Gregory, D.M., Long, D., Morton, A.C., 1990. The Biostratigraphy and Chronostratigraphy of BGS Borehole 78/4, vol. 26. North Minch. SJG, pp. 65–75. https://doi.org/10.1144/sjg26020065.
Guan, H., Liu, L., Hu, Y., Li, S., Li, N., Sun, Z., Wu, N., Somerville, I., 2022. Rising bottom-water temperatures induced methane release during the middle Holocene in the Okinawa trough, East China Sea. Chem. Geol. 590, 120707. https://doi.org/10.1016/j.chemgeo.2022.120707.
Gyllencreutz, R., 2005. Late glacial and Holocene paleoceanography in the Skagerrak from high-resolution grain size records. Palaeogeogr. Palaeoclimatol. Palaeoecol. 222, 344–369. https://doi.org/10.1016/j.palaeo.2005.03.025.
Häkkinen, S., Rhines, P.B., 2004. Decline of subpolar north Atlantic circulation during the 1990s. Science 304, 555–559. https://doi.org/10.1126/science.1094917.
Hald, M., Korsun, S., 1997. Distribution of modern benthic Foraminifera from fjords of Svalbard, European arctic. Journal of Foraminiferal Research - J FORAMIN RES 27, 101–122. https://doi.org/10.2113/gsjfr.27.2.101.
Hald, M., Steinsund, P.I., Dokken, T., Korsun, S., Polyak, L., Aspeli, R., 1994. Recent and late Quaternary distribution of Elphidium excavatum F. Clavatum in arctic seas. In: Sejrup, H.P., Knudsen, K.L. (Eds.), Late Cenozoic Benthic Foraminifera: Taxonomy, Ecology and Stratigraphy. in Honour of Rolf W. Feyling-Hanssen on his 75th Birthday. Cushman Foundation for Foraminiferal Research, 0. (Accessed 24 July 1993).
Harvey, J., Arhan, M., 1988. The Water Masses of the Central North Atlantic in 1983—84.
Hátún, H., Azetsu-Scott, K., Somavilla, R., Rey, F., Johnson, C., Mathis, M., Mikolajewicz, U., Coupel, P., Tremblay, J.-É., Hartman, S., Pacariz, S.V., Salter, I., Ólafsson, J., 2017. The subpolar gyre regulates silicate concentrations in the north Atlantic. Sci. Rep. 7, 14576. https://doi.org/10.1038/s41598-017-14837-4.
Hátún, H., Larsen, K.M.H., Eliasen, S.K., Mathis, M., 2021. Major nutrient fronts in the northeastern Atlantic: from the subpolar gyre to adjacent shelves. In: Belkin, I.M. (Ed.), Chemical Oceanography of Frontal Zones, the Handbook of Environmental Chemistry. Springer, Berlin Heidelberg, Berlin, Heidelberg, pp. 97–141. https://doi.org/10.1007/698_2021_794.
Hátún, H., Sandø, A.B., Drange, H., Hansen, B., Valdimarsson, H., 2005. Influence of the Atlantic subpolar gyre on the thermohaline circulation. Science 309, 1841–1844. https://doi.org/10.1126/science.1114777.
Haynes, J.R., 1973. Cardigan Bay recent foraminifera (cruises of the R. V. Antur, 1962-1964). Bulletin of the British museum (natural history). Zoology. Supplement Supplement 4, 1–245. https://doi.org/10.5962/p.312693.
Hayward, B.W., Grenfell, H.R., Sabaa, A.T., Neil, H.L., 2007. Factors influencing the distribution of Subantarctic deep-sea benthic Foraminifera, campbell and bounty plateaux, New Zealand. Mar. Micropaleontol. 62, 141–166. https://doi.org/10.1016/j.marmicro.2006.08.001.
Heaton, T.J., Butzin, M., Bard, E., Ramsey, C.B., Hughen, K.A., Köhler, P., Reimer, P.J., 2023. Marine radiocarbon calibration in polar regions: a simple approximate approach using MARINE20. Radiocarbon 65, 848–875. https://doi.org/10.1017/RDC.2023.42.
Heaton, T.J., Köhler, P., Butzin, M., Bard, E., Reimer, R.W., Austin, W.E.N., Ramsey, C.B., Grootes, P.M., Hughen, K.A., Kromer, B., Reimer, P.J., Adkins, J., Burke, A., Cook, M. S., Olsen, J., Skinner, L.C., 2020. Marine20—The marine radiocarbon age calibration curve (0–55,000 cal BP). Radiocarbon 62, 779–820. https://doi.org/10.1017/RDC.2020.68.
Herbaut, C., Houssais, M.-N., 2009. Response of the eastern north Atlantic subpolar gyre to the north Atlantic oscillation. Geophys. Res. Lett. 36. https://doi.org/10.1029/2009GL039090.
Holliday, N.P., 2003. Air-sea interaction and circulation changes in the northeast Atlantic. J. Geophys. Res.: Oceans 108. https://doi.org/10.1029/2002JC001344.
Holliday, N.P., Hughes, S.L., Bacon, S., Beszczynska-Möller, A., Hansen, B., Lavín, A., Loeng, H., Mork, K.A., Østerhus, S., Sherwin, T., Walczowski, W., 2008. Reversal of the 1960s to 1990s freshening trend in the northeast north Atlantic and nordic seas. Geophys. Res. Lett. 35. https://doi.org/10.1029/2007GL032675.
Holt, J., Butenschön, M., Wakelin, S.L., Artioli, Y., Allen, J.I., 2012. Oceanic controls on the primary production of the northwest european Continental shelf: model experiments under recent past conditions and a potential future scenario. Biogeosciences 9, 97–117. https://doi.org/10.5194/bg-9-97-2012.
Holt, J., Polton, J., Huthnance, J., Wakelin, S., O’Dea, E., Harle, J., Yool, A., Artioli, Y., Blackford, J., Siddorn, J., Inall, M., 2018. Climate-driven change in the north Atlantic and arctic oceans can greatly reduce the circulation of the north sea. Geophys. Res. Lett. 45 (11). https://doi.org/10.1029/2018GL078878, 827-11,836.
Hoogakker, B., Ishimura, T., de Nooijer, L., Rathburn, A., Schmiedl, G., 2024. A review of benthic foraminiferal oxygen and carbon isotopes. Quat. Sci. Rev. 342, 108896. https://doi.org/10.1016/j.quascirev.2024.108896.
Hulme, P.D., Shirriffs, J., 1994. The late-glacial and Holocene vegetation of the lang lochs mire area, gulberwick, shetland: a pollen and macrofossil investigation. New Phytol. 128, 793–806. https://doi.org/10.1111/j.1469-8137.1994.tb04040.x.
Hurrell, J.W., 1995. Decadal trends in the north Atlantic oscillation: regional temperatures and precipitation. Science 269, 676–679. https://doi.org/10.1126/science.269.5224.676.
Huthnance, J., Weisse, R., Wahl, T., Thomas, H., Pietrzak, J., Souza, A.J., van Heteren, S., Schmelzer, N., van Beusekom, J., Colijn, F., Haigh, I., Hjøllo, S., Holfort, J., Kent, E. C., Kühn, W., Loewe, P., Lorkowski, I., Mork, K.A., Pätsch, J., Quante, M., Salt, L., Siddorn, J., Smyth, T., Sterl, A., Woodworth, P., 2016. Recent change—north sea. In: Quante, M., Colijn, F. (Eds.), North Sea Region Climate Change Assessment. Springer International Publishing, Cham, pp. 85–136. https://doi.org/10.1007/978-3-319-39745-0_3.
Jansen, E., Andersson, C., Moros, M., Nisancioglu, K.H., Nyland, B.F., Telford, R.J., 2008. The early to mid-holocene thermal optimum in the north Atlantic. In: Natural Climate Variability and Global Warming. John Wiley & Sons, Ltd, pp. 123–137. https://doi.org/10.1002/9781444300932.ch5.
Jennings, A.E., Weiner, N.J., Helgadottir, G., Andrews, J.T., 2004. Modern foraminiferal faunas of the southwestern to northern Iceland shelf: oceanographic and environmental controls. J. Foraminifer. Res. 34, 180–207. https://doi.org/10.2113/34.3.180.
Johnson, C., Inall, M., Häkkinen, S., 2013. Declining nutrient concentrations in the northeast Atlantic as a result of a weakening subpolar gyre. Deep Sea Res. Oceanogr. Res. Pap. 82, 95–107. https://doi.org/10.1016/j.dsr.2013.08.007.
Kaufman, D., McKay, N., Routson, C., Erb, M., Dätwyler, C., Sommer, P.S., Heiri, O., Davis, B., 2020. Holocene global mean surface temperature, a multi-method reconstruction approach. Sci. Data 7, 201. https://doi.org/10.1038/s41597-020-0530-7.
Kazuhiro, K., Ashi, J., Yokoyama, Y., Miyairi, Y., Kuramoto, S., 2016. Analysis of past recurrent methane seep activity using radiocarbon dating of calyptogena spp. shells in the eastern nankai subduction zone, Japan. Presented at the EGU General Assembly 2016.
Kingsbury, M.V., 2017. A Multiproxy Palaeolimnological Reconstruction of the Nature and Timing of Climatic Changes in the Northern Isles from the End of the Last Glaciation Through the Early Holocene. University of Stirling.
Kissel, C., Van Toer, A., Laj, C., Cortijo, E., Michel, E., 2013. Variations in the strength of the north Atlantic bottom water during Holocene. Earth Planet Sci. Lett. 369–370, 248–259. https://doi.org/10.1016/j.epsl.2013.03.042.
Klitgaard-Kristensen, D., Sejrup, H.F., Haflidason, H., 2002. Distribution of recent calcareous benthic Foraminifera in the northern north sea and relation to the environment. Polar Res. 21, 275–282. https://doi.org/10.1111/j.1751-8369.2002.tb00081.x.
Klitgaard-Kristensen, D., Sejrup, H.P., Haflidason, H., 2001. The last 18 kyr fluctuations in Norwegian Sea surface conditions and implications for the magnitude of climatic change: evidence from the north sea. Paleoceanography 16, 455–467. https://doi.org/10.1029/1999PA000495.
Knudsen, K.L., Stabell, B., Seidenkrantz, M.-S., Eiríksson, J., Blake Jr,, W., 2008. Deglacial and Holocene conditions in northernmost baffin Bay: sediments, Foraminifera, diatoms and stable isotopes. Boreas 37, 346–376. https://doi.org/10.1111/j.1502-3885.2008.00035.x.
Korsun, S., Hald, M., 1998. Modern benthic foraminifera off novaya zemlya tidewater glaciers. Russian Arctic. Arctic and Alpine Research 30, 61–77. https://doi.org/10.1080/00040851.1998.12002876.
Korsun, S.A., Pogodina, I.A., Forman, S.L., Lubinski, D.J., 1995. Recent Foraminifera in glaciomarine sediments from three arctic fjords of novaja zemlja and Svalbard. Polar Res. 14, 15–32. https://doi.org/10.3402/polar.v14i1.6648.
Koul, V., Schrum, C., Düsterhus, A., Baehr, J., 2019. Atlantic inflow to the north sea modulated by the subpolar gyre in a historical simulation with MPI-ESM. J. Geophys. Res.: Oceans 124, 1807–1826. https://doi.org/10.1029/2018JC014738.
Koul, V., Tesdal, J.-E., Bersch, M., Hátún, H., Brune, S., Borchert, L., Haak, H., Schrum, C., Baehr, J., 2020. Unraveling the choice of the north Atlantic subpolar gyre index. Sci. Rep. 10, 1005. https://doi.org/10.1038/s41598-020-57790-5.
Lo Giudice Cappelli, E., Austin, W.E.N., 2020. Marine bivalve feeding strategies and radiocarbon ages in northeast Atlantic coastal waters. Radiocarbon 62, 107–125. https://doi.org/10.1017/RDC.2019.68.
Lo Giudice Cappelli, E., Austin, W.E.N., 2019. Size matters: analyses of benthic foraminiferal assemblages across differing size fractions. Front. Mar. Sci. 6.
Lo Giudice Cappelli, E., Clarke, J.L., Smeaton, C., Davidson, K., Austin, W.E.N., 2019. Organic-carbon-rich sediments: benthic Foraminifera as bio-indicators of depositional environments. Biogeosciences 16, 4183–4199. https://doi.org/10.5194/bg-16-4183-2019.
Lohmann, K., Drange, H., Bentsen, M., 2009. Response of the north Atlantic subpolar gyre to persistent north Atlantic oscillation like forcing. Clim. Dyn. 32, 273–285. https://doi.org/10.1007/s00382-008-0467-6.
Mackensen, A., Schmiedl, G., Harloff, J., Giese, M., 1995. Deep-sea Foraminifera in the south Atlantic Ocean; ecology and assemblage generation. Micropaleontology 41, 342–358.

Martins, V., Dubert, J., Jouanneau, J.-M., Weber, O., da Silva, E.F., Patinha, C., Alveirinho Dias, J.M., Rocha, F., 2007. A multiproxy approach of the Holocene evolution of shelf–slope circulation on the NW iberian Continental shelf. Mar. Geol. 239, 1–18. https://doi.org/10.1016/j.margeo.2006.11.001.

McIntyre, C.P., Wacker, L., Haghipour, N., Blattmann, T.M., Fahrni, S., Usman, M., Eglinton, T.I., Synal, H.-A., 2017. Online 13C and 14C gas measurements by EA-IRMS–AMS at ETH Zürich. Radiocarbon 59, 893–903. https://doi.org/10.1017/RDC.2016.68.

Melaniuk, K., Sztybor, K., Treude, T., Sommer, S., Rasmussen, T.L., 2022. Influence of methane seepage on isotopic signatures in living deep-sea benthic Foraminifera. 79° N. Sci Rep 12, 1169. https://doi.org/10.1038/s41598-022-05175-1.

Mojtahid, M., Schweizer, M., Douarin, M., Gabriel, J., Colin, C., Tisnérat-Laborde, N., Elliot, M., 2021. From glacial times to late Holocene: benthic foraminiferal assemblages from cold water coral habitats off northwest Scotland. Mar. Geol. 440, 106581. https://doi.org/10.1016/j.margeo.2021.106581.

Montgomery, J., Beaumont, J., Jay, M., Keefe, K., Gledhill, A.R., Cook, G.T., Dockrill, S. J., Melton, N.D., 2013. Strategic and sporadic marine consumption at the onset of the Neolithic: increasing temporal resolution in the isotope evidence. Antiquity 87, 1060–1072. https://doi.org/10.1017/S0003598X00049863.

Murray, J.W., 2003a. An illustrated guide to the benthic Foraminifera of the hebridean shelf, west of Scotland, with notes on their mode of life. Palaeontol. Electron. 5, 31, 1.

Murray, J.W., 2004. The Holocene palaeoceanographic history of muck deep, Hebridean shelf, Scotland: has there been a change of wave climate in the past 12 000 years? J. Micropalaeontol. 23, 153–161. https://doi.org/10.1144/jm.23.2.153.

Murray, J.W., 2006. Ecology and Applications of Benthic Foraminifera. Cambridge University Press, Cambridge. https://doi.org/10.1017/CBO9780511535529.

Murray, J.W., 2003b. Foraminiferal assemblage formation in depositional sinks on the Continental shelf west of Scotland. J. Foraminifer. Res. 33, 101–121. https://doi.org/10.2113/0330101.

Murray, J.W., 1991. Ecology and Palaeoecology of Benthic Foraminifera. Longman Scientific and Technical.

New, A.L., Smythe-Wright, D., 2001. Aspects of the circulation in the rockall trough. Continental Shelf Research, The Marine Environment of the North East Atlantic Margin 21, 777–810. https://doi.org/10.1016/S0278-4343(00)00113-8.

Núñez-Riboni, I., Akimova, A., 2017. Quantifying the impact of the major driving mechanisms of inter-annual variability of salinity in the north sea. Prog. Oceanogr. 154, 25–37. https://doi.org/10.1016/j.pocean.2017.04.004.

Oksanen, J., Simpson, G.L., Blanchet, F.G., Kindt, R., Legendre, P., Minchin, P.R., O'Hara, R.B., Solymos, P., Stevens, M.H.H., Szoecs, E., Wagner, H., Barbour, M., Bedward, M., Bolker, B., Borcard, D., Carvalho, G., Chirico, M., Caceres, M.D., Durand, S., Evangelista, H.B.A., FitzJohn, R., Friendly, M., Furneaux, B., Hannigan, G., Hill, M.O., Lahti, L., McGlinn, D., Ouellette, M.-H., Cunha, E.R., Smith, T., Stier, A., Braak, C.J.F.T., Weedon, J., 2024. Vegan: Community Ecology Package.

Olsen, J., Anderson, N.J., Knudsen, M.F., 2012. Variability of the north Atlantic oscillation over the past 5,200 years. Nat. Geosci. 5, 808–812. https://doi.org/10.1038/ngeo1589.

Ouellet-Bernier, M.-M., de Vernal, A., Hillaire-Marcel, C., Moros, M., 2014. Paleoceanographic changes in the disko bugt area, west Greenland, during the Holocene. Holocene 24, 1573–1583. https://doi.org/10.1177/0959683614544060.

Pados-Dibattista, T., Pearce, C., Detlef, H., Bendtsen, J., Seidenkrantz, M.-S., 2022. Holocene palaeoceanography of the northeast Greenland shelf. Clim. Past 18, 103–127. https://doi.org/10.5194/cp-18-103-2022.

Panieri, G., James, R.H., Camerlenghi, A., Westbrook, G.K., Consolaro, C., Cacho, I., Cesari, V., Cervera, C.S., 2014. Record of methane emissions from the West Svalbard continental margin during the last 23.500 yrs revealed by δ13C of benthic Foraminifera. Global Planet. Change 122, 151–160. https://doi.org/10.1016/j.gloplacha.2014.08.014.

Pätsch, J., Gouretski, V., Hinrichs, I., Koul, V., 2020. Distinct mechanisms underlying interannual to decadal variability of observed salinity and nutrient concentration in the northern north sea. J. Geophys. Res.: Oceans 125, e2019JC015825. https://doi.org/10.1029/2019JC015825.

Patterson, R.T., Guilbault, J.-P., Thomson, R.E., 2000. Oxygen level control on foraminiferal distribution in EFFINGHAM inlet, vancouver island, BRITISH columbia, Canada. J. Foraminifer. Res. 30, 321–335. https://doi.org/10.2113/0300321.

Peacock, J.D., Horne, D.J., Whittaker, J.E., 2012. Late devensian evolution of the marine offshore environment of Western Scotland. PGA (Proc. Geol. Assoc.) 123, 419–437. https://doi.org/10.1016/j.pgeola.2012.02.005.

Polyak, L., Korsun, S., Febo, L.A., Stanovoy, V., Khusid, T., Hald, M., Paulsen, B.E., Lubinski, D.J., 2002. Benthic foraminiferal assemblages from the southern kara sea, a river-influenced arctic marine environment. J. Foraminifer. Res. 32, 252–273. https://doi.org/10.2113/32.3.252.

Quintela, M., Costa, P.J.M., Fatela, F., Drago, T., Hoska, N., Andrade, C., Freitas, M.C., 2016. The AD 1755 tsunami deposits onshore and offshore of algarve (south Portugal): sediment transport interpretations based on the study of foraminifera assemblages. Quaternary International, QuicklakeH Special Issue: Rapidly changing large lakes and human response 408, 123–138. https://doi.org/10.1016/j.quaint.2015.12.029.

Rasmussen, S.O., Andersen, K.K., Svensson, A.M., Steffensen, J.P., Vinther, B.M., Clausen, H.B., Siggaard-Andersen, M.-L., Johnsen, S.J., Larsen, L.B., Dahl-Jensen, D., Bigler, M., Röthlisberger, R., Fischer, H., Goto-Azuma, K., Hansson, M.E., Ruth, U., 2006. A new Greenland ice core chronology for the last glacial termination. J. Geophys. Res. Atmos. 111. https://doi.org/10.1029/2005JD006079.

Read, J.F., 2000. CONVEX-91: water masses and circulation of the northeast Atlantic subpolar gyre. Prog. Oceanogr. 48, 461–510. https://doi.org/10.1016/S0079-6611(01)00011-8.

Reimer, P.J., Reimer, R.W., 2001. A marine reservoir correction database and On-Line interface. Radiocarbon 43, 461–463. https://doi.org/10.1017/S0033822200038339.

Roberts, D.H., Evans, D.J.A., Callard, S.L., Clark, C.D., Bateman, M.D., Medialdea, A., Dove, D., Cotterill, C.J., Saher, M., Cofaigh, C.Ó., Chiverrell, R.C., Moreton, S.G., Fabel, D., Bradwell, T., 2018. Ice marginal dynamics of the last British-Irish ice sheet in the southern north sea: ice limits, timing and the influence of the Dogger Bank. Quat. Sci. Rev. 198, 181–207. https://doi.org/10.1016/j.quascirev.2018.08.010.

Roberts, D.H., Grimoldi, E., Callard, L., Evans, D.J.A., Clark, C.D., Stewart, H.A., Dove, D., Saher, M., Ó Cofaigh, C., Chiverrell, R.C., Bateman, M.D., Moreton, S.G., Bradwell, T., Fabel, D., Medialdea, A., 2019. The mixed-bed glacial landform imprint of the north sea lobe in the Western north sea. Earth Surf. Process. Landf. 44, 1233–1258. https://doi.org/10.1002/esp.4569.

Robinson, M., 2004. A late glacial and Holocene diatom record from clettnadal, shetland islands, northern Scotland. J. Paleolimnol. 31, 295–319. https://doi.org/10.1023/B:JOPL.0000021716.49552.da.

Rodrigues, C.G., Hooper, K., 1982. The ecological significance of Elphidium clavatum in the gulf of St. Lawrence, Canada. J. Paleontol. 56, 410–422.

Russell, N., Cook, G.T., Ascough, P.L., Scott, E.M., 2015. A period of calm in Scottish seas: a comprehensive study of ΔR values for the northern British isles coast and the consequent implications for archaeology and oceanography. Quat. Geochronol. 30, 34–41. https://doi.org/10.1016/j.quageo.2015.08.001.

Sarafanov, A., 2009. On the effect of the north Atlantic oscillation on temperature and salinity of the subpolar north Atlantic intermediate and deep waters. ICES (Int. Counc. Explor. Sea) J. Mar. Sci. 66, 1448–1454. https://doi.org/10.1093/icesjms/fsp094.

Schmiedl, G., Mackensen, A., Müller, P.J., 1997. Recent benthic Foraminifera from the eastern south Atlantic Ocean: dependence on food supply and water masses. Mar. Micropaleontol. 32, 249–287. https://doi.org/10.1016/S0377-8398(97)00023-6.

Schönfeld, J., 2002. A new benthic foraminiferal proxy for near-bottom current velocities in the Gulf of Cadiz, northeastern Atlantic Ocean. Deep Sea Res. Oceanogr. Res. Pap. 49, 1853–1875. https://doi.org/10.1016/S0967-0637(02)00088-2.

Schröder, C., 1988. Subsurface Preservation Of Agglutinated Foraminifera In The Northwest Atlantic Ocean.

Scott, G., Scourse, J.D., Austin, W.E.N., 2003. The distribution of benthic foraminifera in the Celtic sea: the significance of seasonal stratification. J. Foraminifer. Res. 33, 32–61.

Scourse, J.D., Afrifa, K., Byrne, L., Crowley, D., Earland, J., Ehmen, T., Frøslev, T., Greenall, C., Harland, J., Heard, Z., Höche, N., Holman, L., Huang, Q., Langkjær, E., Mason, M., Nelson, E., Nemeth, Z., Reynolds, D., Robson, H., Roman Gonzalez, A., Scherer, P., Scolding, J., Short, J., Wilkin, J., Wilson, D., 2022. RRS Discovery DY150 Cruise Summary Report.

Scourse, J.D., Austin, W.E.N., Long, B.T., Assinder, D.J., Huws, D., 2002. Holocene evolution of seasonal stratification in the Celtic sea: refined age model, mixing depths and foraminiferal stratigraphy. Mar. Geol. 191, 119–145. https://doi.org/10.1016/S0025-3227(02)00528-5.

Scourse, J.D., Kennedy, H., Scott, G.A., Austin, W.E.N., 2004. Stable isotopic analyses of modern benthic Foraminifera from seasonally stratified shelf seas: Disequilibria and the "seasonal effect.". Holocene 14, 747–758. https://doi.org/10.1191/0959683604hl753rp.

Seidenkrantz, M.-S., 2013. Benthic Foraminifera as palaeo sea-ice indicators in the subarctic realm – examples from the labrador sea–baffin Bay region. Quaternary Science Reviews, Sea Ice in the Paleoclimate System: the Challenge of Reconstructing Sea Ice from Proxies 79, 135–144. https://doi.org/10.1016/j.quascirev.2013.03.014.

Sejrup, H.-P., Guilbault, J.-P., 1980. Cassidulina reniforme and C. obtusa (foraminifera), taxonomy, distribution, and ecology. Sarsia 65, 79–85. https://doi.org/10.1080/00364827.1980.10431476.

Shackleton, N., 1974. Attainment of Isotopic Equilibrium Between Ocean Water and the Benthonic Foraminifera Genus Uvigerina: Isotopic Changes in the Ocean During the Last Glacial.

Shannon, C.E., Weaver, W., 1949. The mathematical theory of communication. M Comput. 27, 306–317.

Sheehan, P., Berx, B., Gallego, A., Hall, R., Heywood, K., Hughes, S., 2017. Thermohaline forcing and interannual variability of northwestern inflows into the northern north sea. Cont. Shelf Res. 138. https://doi.org/10.1016/j.csr.2017.01.016.

Sheridan, A., 2012. Neolithic shetland: a view from the "mainland.". The border of farming and the cultural markers 6–36.

Sherwin, T.J., Read, J.F., Holliday, N.P., Johnson, C., 2012. The impact of changes in north Atlantic gyre distribution on water mass characteristics in the rockall trough. ICES (Int. Counc. Explor. Sea) J. Mar. Sci. 69, 751–757. https://doi.org/10.1093/icesjms/fsr185.

Smedile, A., De Martini, P.M., Pantosti, D., 2012. Combining inland and offshore paleotsunamis evidence: the Augusta Bay (eastern sicily, Italy) case study. Nat. Hazards Earth Syst. Sci. 12, 2557–2567. https://doi.org/10.5194/nhess-12-2557-2012.

Solignac, S., Grelaud, M., de Vernal, A., Giraudeau, J., Moros, M., McCave, I.N., Hoogakker, B., 2008. Reorganization of the upper ocean circulation in the mid-Holocene in the northeastern AtlanticThis article is one of a series of papers published in this special issue on the theme Polar climate stability Network.GEOTOP publication 2009-0002. Can. J. Earth Sci. 45, 1417–1433. https://doi.org/10.1139/E08-061.

Staines-Urías, F., Kuijpers, A., Korte, C., 2013. Evolution of subpolar north Atlantic surface circulation since the early Holocene inferred from planktic Foraminifera faunal and stable isotope records. Quat. Sci. Rev. 76, 66–81. https://doi.org/10.1016/j.quascirev.2013.06.016.

Stuiver, M., Polach, H.A., 1977. Discussion reporting of 14C data. Radiocarbon 19, 355–363. https://doi.org/10.1017/S0033822200003672.

Stuiver, M., Reimer, P.J., 1993. CALIB rev. 8. Radiocarbon 35, 215–230.

Thornalley, D.J.R., Blaschek, M., Davies, F.J., Praetorius, S., Oppo, D.W., McManus, J.F., Hall, I.R., Kleiven, H., Renssen, H., McCave, I.N., 2013. Long-term variations in Iceland–Scotland overflow strength during the Holocene. Clim. Past 9, 2073–2084. https://doi.org/10.5194/cp-9-2073-2013.

Thornalley, D.J.R., Elderfield, H., McCave, I.N., 2009. Holocene oscillations in temperature and salinity of the surface subpolar north Atlantic. Nature 457, 711–714. https://doi.org/10.1038/nature07717.

Turrell, W.R., 1992. The East Shetland Atlantic Inflow, pp. 127–143. Dickson RR, et al 1980–1989.

Turrell, W.R., Slesser, G., Payne, R., Adams, R.D., Gillibrand, P.A., 1996. Hydrography of the east shetland basin in relation to decadal north sea variability. ICES (Int. Counc. Explor. Sea) J. Mar. Sci. 53, 899–916. https://doi.org/10.1006/jmsc.1996.0112.

van der Molen, J., Pätsch, J., 2022. An overview of Atlantic forcing of the north sea with focus on oceanography and biogeochemistry. J. Sea Res. 189, 102281. https://doi.org/10.1016/j.seares.2022.102281.

Van Nieuwenhove, N., Pearce, C., Knudsen, M.F., Røy, H., Seidenkrantz, M.-S., 2018. Meltwater and seasonality influence on subpolar gyre circulation during the Holocene. Palaeogeogr. Palaeoclimatol. Palaeoecol. 502, 104–118. https://doi.org/10.1016/j.palaeo.2018.05.002.

Ward, S.L., Bradley, S.L., Roseby, Z.A., 2025a. Dataset: the role of long-term hydrodynamic evolution in the accumulation and preservation of organic carbon-rich deposits in the shelf seas. https://doi.org/10.5281/zenodo.14795629.

Ward, S.L., Bradley, S.L., Roseby, Z.A., Wilmes, S.-B., Vosper, D.F., Roberts, C.M., Scourse, J.D., 2025b. The role of long-term hydrodynamic evolution in the accumulation and preservation of organic carbon-rich shelf sea deposits. J. Geophys. Res.: Oceans 130, e2024JC022092. https://doi.org/10.1029/2024JC022092.

Whittington, G., Buckland, P., Edwards, K.J., Greenwood, M., Hall, A.M., Robinson, M., 2003. Multiproxy devensian late-glacial and Holocene environmental records at an Atlantic coastal site in shetland. J. Quat. Sci. 18, 151–168. https://doi.org/10.1002/jqs.746.

Whittington, Graeme, Edwards, K.J., 1993. Vegetation change on papa stour, shetland, Scotland: a response to coastal evolution and human interference? Holocene 3, 54–62. https://doi.org/10.1177/095968369300300106.

Winther, N.G., Johannessen, J.A., 2006. North sea circulation: atlantic inflow and its destination. J. Geophys. Res.: Oceans 111. https://doi.org/10.1029/2005JC003310.

Witbaard, R., 1996. Growth variations in arctica islandica L. (mollusca): a reflection of hydrography-related food supply. ICES (Int. Counc. Explor. Sea) J. Mar. Sci. 53, 981–987. https://doi.org/10.1006/jmsc.1996.0122.

Woods, M.A., Wilkinson, I.P., Leng, M.J., Riding, J.B., Vane, C.H., Lopes dos Santos, R.A., Kender, S., De Schepper, S., Hennissen, J.A.I., Ward, S.L., Gowing, C.J.B., Wilby, P. R., Nichols, M.D., Rochelle, C.A., 2019. Tracking Holocene palaeostratification and productivity changes in the Western Irish sea: a multi-proxy record. Palaeogeogr. Palaeoclimatol. Palaeoecol. 532, 109231. https://doi.org/10.1016/j.palaeo.2019.06.004.